University College of Southeast Norway
Faculty of Technology, Natural Sciences and Maritime Sciences

Doctoral dissertation no. 27
2017

Luca Marchetti

Design of a bidirectional front-end for resonating sensors

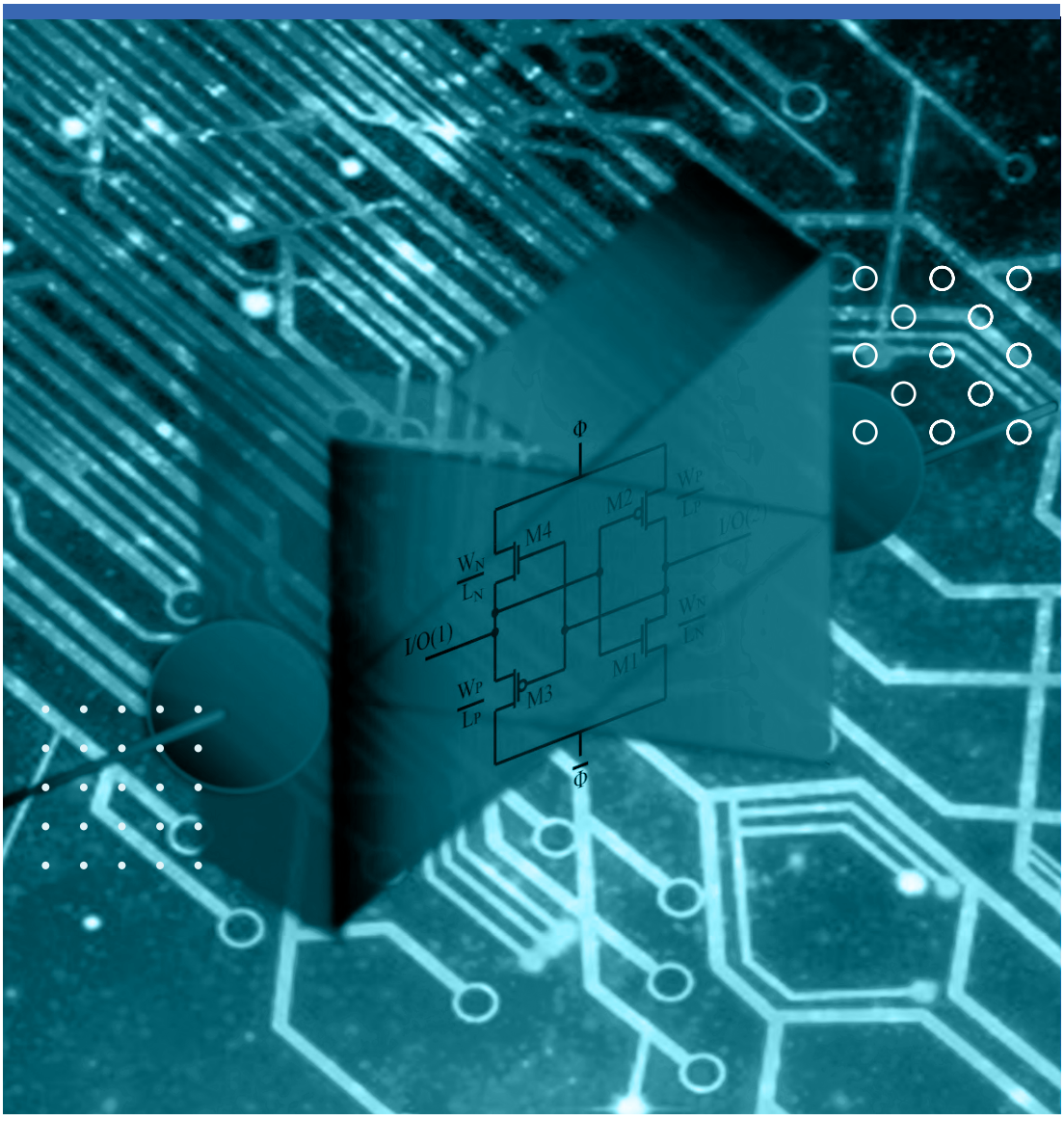

HSN

Luca Marchetti

Design of a bidirectional front-end for resonating sensors

A PhD dissertation in
Applied Micro- and Nanosystems

Faculty of Technology, Natural Sciences and Maritime Sciences
University College of Southeast Norway
Kongsberg, 2017

Doctoral dissertations at the University College of Southeast Norway no. 27

ISSN: 2464-2770 (print)
ISSN: 2464-2483 (electronic)
ISBN: 978-82-7860-306-2 (print)
ISBN: 978-82-7860-307-9 (electronic)

Print: University College of Southeast Norway

Dedication

This dissertation is dedicated to my family, their support, encouragement and constant love have sustained during all my student career. Their good examples have taught me to work hard for the things that I aspire to achieve. I also dedicate this work to my girlfriend who supported me with constant encouragement throughout the last period of this PhD.

Acknowledgements

I wish, first and foremost, to express my sincere gratitude to my supervisor Mehdi Azadmehr for his continuous commitment to help and believing in me during all my PhD career. He gave me much valuable knowledge about what means to become a researcher in this field. With his guidance, and his supporting words helped me to look always forward without any fear. I really thank him for giving me the opportunity to research about such interesting topic. I am thankful also to my co-supervisors Omid Mirmotahari and Yngvar Berg who gave me good suggestions and support whenever I needed. I would like to thank Tor Olaf Berger who gave me valuable assistance in the laboratory, every time I had to perform measurements or during the fabrication of electronic circuits. Finally, I would like to thank again my family, my girlfriend and whoever supported me during all my PhD career.

Abstract

In the last decades, the use of electronic sensors in portable applications became increasingly common. They provide a simple way to study processes, monitor environment conditions or to provide hazard systems. In order to interpret the signals generated by these sensors correctly, an electronic Front-End must be used to elaborate and translate them into a signal understood by a Processing Unit.

This thesis presents the design of a novel electronic Front-End for resonating sensors, characterized by compactness and simplicity. This Front-End is a purely analog system based on a bidirectional pseudo floating gate amplifier (PFGA). Given the low number of MOSFETs used to implement this amplifier, it is very simple, compact and with potentially low power dissipation. This document exploits the possibility to use the bidirectional behavior of the PFGA to implement an electronic Front-End for resonating sensors. Furthermore, a prototype of a bidirectional PFGA has been realized using commercial component CD4007UBE. A full characterization of this front-end has been developed in this work, from the modeling to the measurements on full functioning prototype. Additional features have been added to the basic structure to improve the front-end such as a control electronic system to lower the power consumption of the amplifier and a technique to control its bandwidth. In conclusion, a comparison with the state of the art shows that the power consumption is comparable with other structures described in the literature but it benefits of a smaller occupation of area.

Keywords: Bidirectional; Amplifier; Front-End; Pseudo-Floating-Gate; Compact; Resonating Sensors.

List of papers

Articles omitted from online edition due to publisher's restrictions

Article 1:

L. Marchetti, A. Romi, Y. Berg, O. Mirmotahari and M. Azadmehr, "A discrete implementation of a bidirectional circuit for actuation and read-out of resonating sensors," 2016 International Conference on Design and Technology of Integrated Systems in Nanoscale Era (DTIS), Istanbul, 2016, pp. 1-5. doi: 10.1109/DTIS.2016.7483896

Article 2:

L. Marchetti, Y. Berg, O. Mirmotahari and M. Azadmehr, "Bidirectional front-end for piezoelectric resonator," 2016 IEEE 13th International Conference on Networking, Sensing, and Control (ICNSC), Mexico City, 2016, pp. 1-4. doi: 10.1109/ICNSC.2016.7479028

Article 3:

L. Marchetti, Y. Berg and M. Azadmehr, "An autozeroing inverter based front-end for resonating sensors," 2017 12th International Conference on Design & Technology of Integrated Systems In Nanoscale Era (DTIS), Palma de Mallorca, 2017, pp. 1-5. doi: 10.1109/DTIS.2017.7930154

Article 4:

L. Marchetti, Y. Berg, O. Mirmotahari and M. Azadmehr, "A control system for a low power bidirectional front-end for resonating sensors," 2017 IEEE 14th International Conference on Networking, Sensing and Control (ICNSC), Calabria, Italy, 2017, pp. 322-326 . doi: 10.1109/ICNSC.2017.8000112

Article 5:

L. Marchetti, Y. Berg and M. Azadmehr, "A Bidirectional Front-End with Bandwidth Control for Actuation and Read-Out of MEMS Resonating Sensors," 2017 24th International Conference Mixed Design of Integrated Circuits and Systems (MIXDES), Bydgoszcz, 2017,

Article 6:

L. Marchetti, Y. Berg and M. Azadmehr, "Analysis of the Effect of Channel Leakage on Design, Characterization and Modelling of a high voltage Pseudo-Floating Gate Sensor-Front-End", accepeted in Electronics MDPI journal

Article 7:

L. Marchetti, Y. Berg and M. Azadmehr, "Design and Modelling of a Bidirectional Front-End for Resonating Sensors based on Pseudo Floating Gate Amplifier", accepted in Electronics MDPI journal

Co-Author of the following publications:

Article 8:

M. Azadmehr, L. Marchetti, Y. Berg "A Low Power Voltage Similarity Circuit," 2017 IEEE 50th International Symposium of Circuits and Systems (ISCAS), Baltimore, 2017

Article 9:

M. Azadmehr, L. Marchetti, Y. Berg, "A Virtual Wheatstone Bridge Front-End for Resistive Sensors," 2017 IEEE 14th International Conference on Networking, Sensing, and Control (ICNSC), Calabria, 2017

List of Figures

Abbreviations

ADC ..... analog to Digital Converter

AFE ..... Analog Front-End

ASIC ..... Application Specific Integrated Circuit

BPFGA ..... Bidirectional Pseudo Floating Gate Amplifier

BVD ..... Butterworth Van Dike

FFT ..... Fast Fourier Transform

HTV-PFGA . High Threshold Voltage Pseudo Floating Gate Amplifier

IA ..... Impedance Analysis

IC ..... Integrated Circuit

LNA ..... Low Noise Amplifier

MEMS ..... Micro-Electro Mechanical System

MOSFET .... Metal Oxide Semiconductor Field Effect Transistor

OBM ..... Oscillator-Based Measurement

OP-AMP .... Operational Amplifier

OTA ..... Operational Trans-conductance Amplifier

PFGA ..... Pseudo Floating Gate Amplifier

RDM ..... Ring-Down Measurement

RLC ..... Resistance-Inductance-Capacitance

List of Symbols

C_F ..... Feedback Capacitance

C_{IN} ..... Input Capacitance

C_E ..... Parasitic Capacitance of the Sensor due to the Electrodes

C_L ..... Load Capacitance

f_{res} ..... Resonant Frequency

k ..... Stiffness

k_p, k_n ..... transconductance parameter of a PMOS or NMOS respectively

m ..... Mass

R_{OFF} ..... Drain-Source OFF Resistance

$R_{o.inv}$ ..... Total Output Resistance of a Digital Inverter

t_{sw} ..... Swapping time of a Bidirectional Pseudo Floating Gate Amplifier

W/L ..... MOSFET Aspect Ratio

V_{DD} ..... Power Supply

V_{RLC} ..... Voltage Across the Sensor

$\Phi, \overline{\Phi}$ ..... Power Supply of a Bidirectional Pseudo Floating Gate Amplifier

Contents

Chapter 1

Introduction and Background

1.1 State of the Art

Recent technological developments in electronic systems have led to an exponential growth in the demand for various types of sensors. Nowadays, sensors are being used in many applications such as environment monitoring [3], medical applications [4], automotive [5] and etc. Furthermore, a rapid progress in MEMS technology [6] allowed to reduce the dimensions of these devices to micro-scale, which makes them easy to include in portable devices. The use of sensors in portable applications, such as cell phones, have slowly became an essential feature, but the design of the whole system introduced new strict requirements regarding the power consumption and the area occupied.

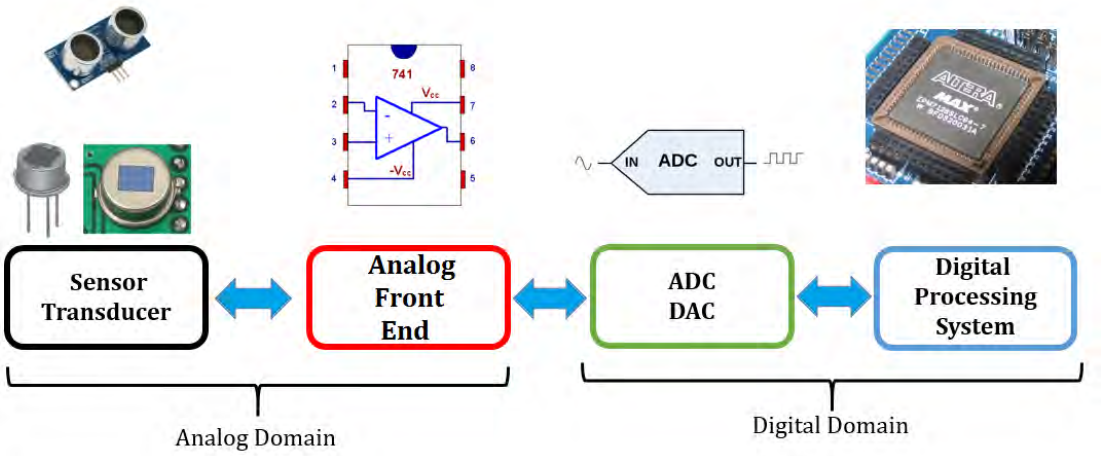

Figure 1.1: Sensor Node Block Diagram

Sensors and their electronic interfaces are known as sensor nodes, which are usually connected in a network. In this way sensor nodes can communicate with each other and a central unit, utilized to process the data acquired from the surrounding environment. The purpose of a sensor network is usually two sided, to study or analyze fundamental processes and/or provide systems, which can detect and respond to particular events that occur in the surrounding environment. The electronic interface of a sensor transforms the signal generated by these devices in a form, which can be easily interpreted by a digital system such as a computer or displayed in an understandable way. A sensor node can be recognized by 4 main building blocks as shown in Fig.1.1: a sensor, an analog electronic front-end (AFE), Analog to Digital Converter (ADC) and a digital processing unit including the communication. The reason of this typical structure is that by using digital signals the elaboration of the measurements can be performed much faster than what it can be done with analog signals, without loosing precision and improving immunity of the system to the noise. The main purpose of the analog electronic front-end is to provide a signal, which is ready to be converted in digital form. This block is often referred to as signal conditioning block and performs operations such as amplification, filtering, level shifting, conversions (ex:I/V) and etc. Once the readability of the signal has been improved, it is possible to perform the conversion to digital form by using an analog to Digital Converter (ADC). Finally, the information can be extracted and processed by a digital signal processor. Sensors are a type of transducer, two terms, which are often used interchangeably. However, in strict sense the definition of transducer is more general.

A sensor is an electronic device that converts a physical quantity into electrical signal, while a transducer converts energy from a form to another. A transducer can be used as sensor, but can be also used as actuator, this explain why the measurement chain in Fig.1.1 is bidirectional. In some applications, the digital processor sends a control signal to actuate the sensor and then performs the measurement. An interesting type of transducer, which falls in this classification and it is also object of this research is the resonating transducer, which transforms electrical to mechanical energy and vice versa. These devices have been studied for long time given their

numerous advantages such as low drift, accuracy and high resolution [7],[8] and they have been applied in many fields such as automotive, health care systems, hazard systems, ultrasound systems and so on (Fig.1.2).

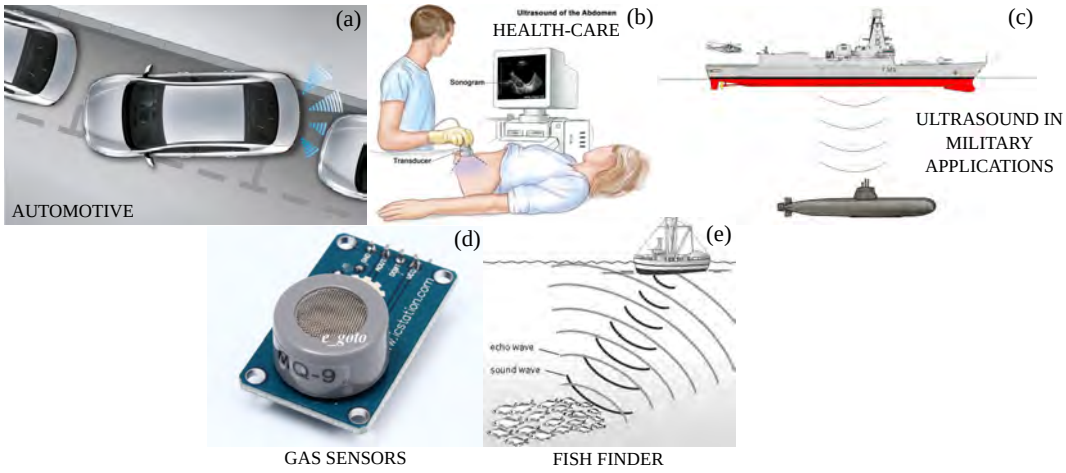

Figure 1.2: Examples of applications for Resonating Sensors. (a) Parking Assistance. (b) Health-Care (c) Military applications. (d) Gas Detectors (e) Fish finders.

Examples of resonating sensors are described in [1],[9]. Resonating sensors need to be actuated and read-out. There are three main techniques to perform a measurement with this type of sensors: Impedance Analysis (IA), Oscillator-Based Measurement (OBM) and Ring-Down Measurement (RDM) [10]. These methods are schematically represented in Fig.1.3.

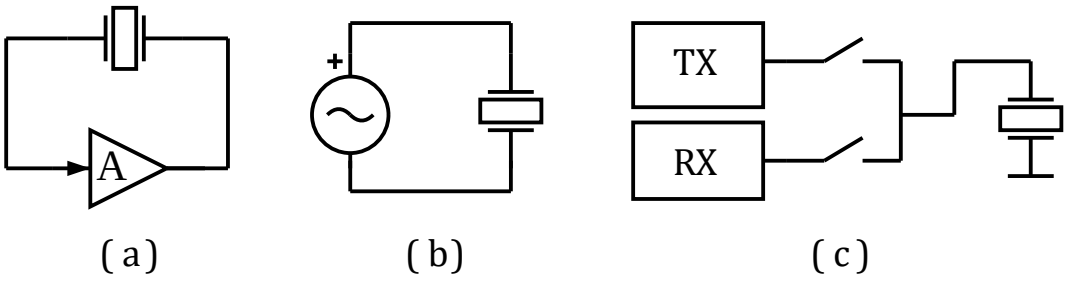

Figure 1.3: State of the Art in Self-Sensing Approaches for Resonating Transducers. (a) Oscillator-Based Method. (b) Impedance Measurement. (c)Ring Down Method.

The IA method is generally slow since it requires a sweep in frequency of the input signal to trace the impedance vs. frequency plot. The OBM method is generally power consuming because the resonating device is used to close a positive feedback loop of an amplifier, which is continuously exciting the transducer. However, the

Ring Down method is a good candidate to implement a low power system. The ring down method is based on two phases: the actuation phase and the read-out phase. During the first phase, an electronic circuit excites the transducer by mean of an electrical signal. The electrical energy provided to the sensor is then converted in mechanical energy in the form of vibration. Finally, in the second phase, another electronic circuit reads the transducer. All of these techniques are also known as self-sensing approaches, which consists of the fact that a transducer is used both as sensor and actuator [11],[12]. In this thesis, the Ring-Down method will be utilized as design strategy to implement a novel Front-End for resonating transducers.

1.2 Motivation

The limited lifetime of the power sources in portable sensors nodes created the need to develop an energy efficient electronic interface to read-out sensors. These power sources are either battery with a limited lifetime or an energy harvester with a limited power, which has to be enough to feed the entire system. Therefore, the aim of this thesis consists in implementing a compact and low power analog Front-End to actuate and read-out resonating sensors. In particular, the Ring Down Method has been chosen as design strategy since it requires a less complex system and can consume less power than the other techniques. This work investigates the possibility to implement this method by using a suitable analog electronic circuit, which can satisfy these requirements. The main concern of this research is to analyze and extract a design procedure for the analog front-end based on a bidirectional pseudo floating gate amplifier (BPFGA), utilized for both actuation and read-out of the resonating sensor. The key point consists in substituting the systems for the actuation and the read-out of the sensor with a bidirectional device, which provides both functions. The PFGA has been proved in literature to be a compact and low power at low supply voltages, but not studied at higher supply values. Since most of the common resonating sensors require an actuation voltage greater than the ones used for traditional low power circuits, the PFGA structure must be re-analyzed in order to describe secondary phenomenon, which were not relevant for lower power supply values. After the PFGA has been re-analyzed, its bidirectional behaviour

will be studied. Finally, this research provide a detail description of the dynamic of the Front-End when connected to a resonating load, emphasizing the differences between the signals obtained when the Front-End is connected to a real sensor and when it is connected to a load, which approximate the behaviour of the resonating sensor. The applications for this novel Front-End will be numerous, but one of the most attractive purposes is the use of this device to drive arrays of transducers for ultrasound imaging due to its compactness.

1.3 Research Contribution

This thesis describes and analyses in detail the working principle of a bidirectional Front-End for resonating sensors based on pseudo floating gate amplifier. This type of front-end has been initially introduced and simulated in [13] and thought to be used as electronic Front-End for MEMS resonant sensors. The concept was proven just through simulations. Therefore, the next step was to realize a prototype, to verify the validity of the Front-End. The system has been proved to be conceptually functional in [14],[15]. In [14] the bidirectional Front-End has been tested with a series RLC circuit, which mimics the behaviour of a resonant transducer, while in [15] the same system has been tested with a real transducer to evaluate the accuracy of the approximated model used. The transducer chosen is a piezoelectric ceramic disk (FERROPERM) with a resonant frequency of 100kHz, since it falls inside the bandwidth of the electronic Front-End. In both publication, the Front-End has been tested with a power supply voltage of 5V, first because it provides a sensor response with a wide amplitude that can be easily monitored by the typical electronic instrumentation (oscilloscope, multimeter,...), second because it falls in the power supply range of the integrated circuit used to implement the Front-End. However, similar results can be obtained by using lower or higher power supply values. In order to reduce the power consumption of the Front-End, a sleeping mode was added. This mode consists in turning off the amplifier after a few periods of the output signal have been read and the resonant frequency has been extracted with a certain accuracy. This system is discussed in detail in [16]. In this publication, the sleeping mode has been activated after reading one period of the oscillation generated by the

sensor, however due to the flexibility of the control system, the sleeping mode can be activated after a configurable number of cycles of this oscillating signal. This method has been proved to be functional, providing a power consumption lower or equal to the ones described in the State of the Art. A further improvement to the basic structure of the bidirectional Front-End has been provided by adding a way to control the bandwidth of the amplifier by simply tuning a bias voltage. This improved circuit is based on a stacked-inverter, which allows to limit the current and varying the output resistance by changing the value of a bias voltage. This is an interesting feature, which allows to increase the signal to noise ratio in the output signal of the Front-End. Further details can be found in [17]. An alternative Bidirectional Front-End based on an auto-zeroing amplifier realized with a logic inverter has been proposed in [18]. This new structure has been developed to compare the performances between an open loop solution and the bidirectional amplifier based on PFGA. Both circuits biasing is based on a parasitic phenomena, leakage currents for the BPFGA and charge stored on the parasitic capacitance of the resonant sensor for the open loop amplifier. In order to have a comprehensive understanding of the design of a BPFGA, a detailed investigation of PFGA has been discussed in [19]. This particular work aimed to provide precise design rules for a PFGA implemented in low leakage CMOS technology and a comparison with an high leakage implementation. These results have been used in another successive work where the dynamic behavior of the BPFGA has been discussed in detail. The work described in [20] has the purpose of providing a detail analysis of the BPFGA and to define precise design rules to drive and read-out a resonant load.

1.4 Dissertation Outline

This thesis is divided in 5 chapters. The first chapter consists of a general introduction about the State of the Art of the Front-End for resonating sensors, the aims of this thesis and the research contribution to the field. The second chapter consists of a brief description of resonating sensors, their working principle, available technologies and modelling. Particular emphasis has been given to the Butterworth Van Dyke (BvD) model, which is also the approximated model for the load used during

this research. Chapter three presents a short introduction of the state of the art of pseudo floating gate amplifiers (PFGA) and its basic principle. Furthermore, a comparison between the performance of a PFGA characterized by low and high leakage currents has been discussed in this chapter. Finally, chapter 4 describes the main topic of this research: the Bidirectional Front-End based on Pseudo Floating gate Amplifier (PFGA). The second part of this chapter describes the added features to the bidirectional amplifier such as sleeping mode, bandwidth control. Furthermore, a comparison between an auto-zeroing amplifier inverter-based and the BPFGA is provided. This thesis ends with conclusions and proposal for future works in chapter 5.

Chapter 2

Resonating Sensors

As the main signal processing in modern control systems is digital, they require sensors, which can provide digital outputs directly. Sensor which have outputs based on frequency or phase changing have the advantage that they can be read directly by a digital system [1] such as the resonating sensor. Furthermore, resonant sensors provide high accuracy, low drift and high resolution [7],[8]. In the next sections, a detailed description of this type of sensors is provided.

2.1 Basic Principle

A resonant transducer converts physical quantities of the surrounded environment into a time varying electrical signal, which can be read-out by an electronic interface. In order to generate the electrical signal, the transducer must be excited electrically, which induces a mechanical vibration in this device. The electro-mechanical coupling of the transducer allows to transform the mechanical perturbation in an electrical oscillation characterized by a particular frequency called resonant frequency. The value of this parameter is directly related to the measurand, therefore once it has been read, it can be used to obtain the information required. The relationship between the measurand and the resonant frequency (f_{res}) is synthesized in Eq.2.1.

$$f_{res} = \frac{1}{2\pi}\sqrt{\frac{k}{m}} \tag{2.1}$$

Where m is the mass and k is the stiffness of the transducer. If a physical

quantity in the surrounding environment changes the mass or the stiffness of the transducer, then the resonant frequency changes. A device such as the resonant transducer characterized by an output in frequency presents 2 major advantages: it is not affected by noise on the amplitude of the oscillating signal and can be digitized easily by counting the periods [21]. Often, the output signal of this type of sensor is referred to as quasi-digital signal. Furthermore, amplitude and phase could be also used to bring information and they are specially used in acoustic applications. In conclusion, a generic resonant sensor can be modelled as a 2 port device: one port is connected to the mechanical domain (input port) and the other port is connected to the electrical domain (output port) as shown in Figure2.1.

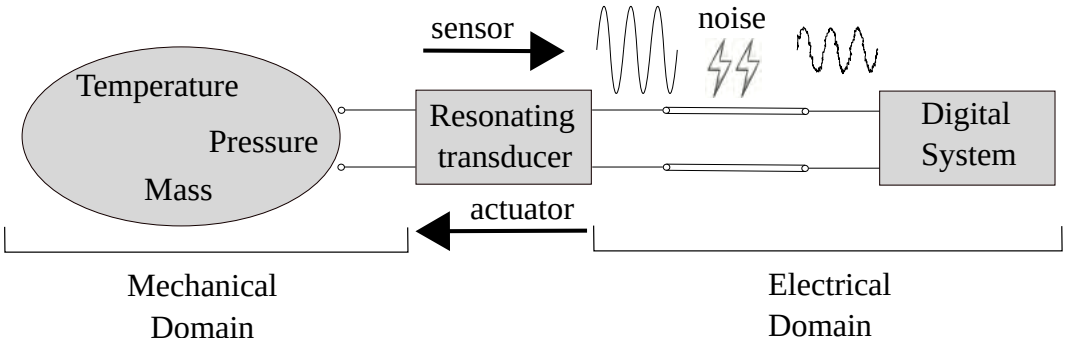

Figure 2.1: Resonating Sensor Diagram Block

A few examples of applications for this device could be: temperature sensor, in which the thermal expansion affects the stiffness of the device, a pressure sensor in which a deformation of the transducer varies the stiffness, a deposition detector based on mass variations of the sensor due to the deposition of a material on it such as gas, micro-droplets, thin layer deposited during MEMS fabrication and etc.

2.2 Discrete and MEMS Resonating Sensors

The fast development in the fabrication and the increased down-scaling of resonating transducers has resulted in a huge variety of this type of sensors. Resonant sensors can be actuated mechanically, electro-statically, electromagnetically, thermally, etc. Some examples of discrete resonant sensors are shown in Fig.2.2.

Fig.2.2(a) shows a resonant sensor, which can detect the density of the liquid inside a pipe based on the resonant frequency of the pipe. An electromagnetic

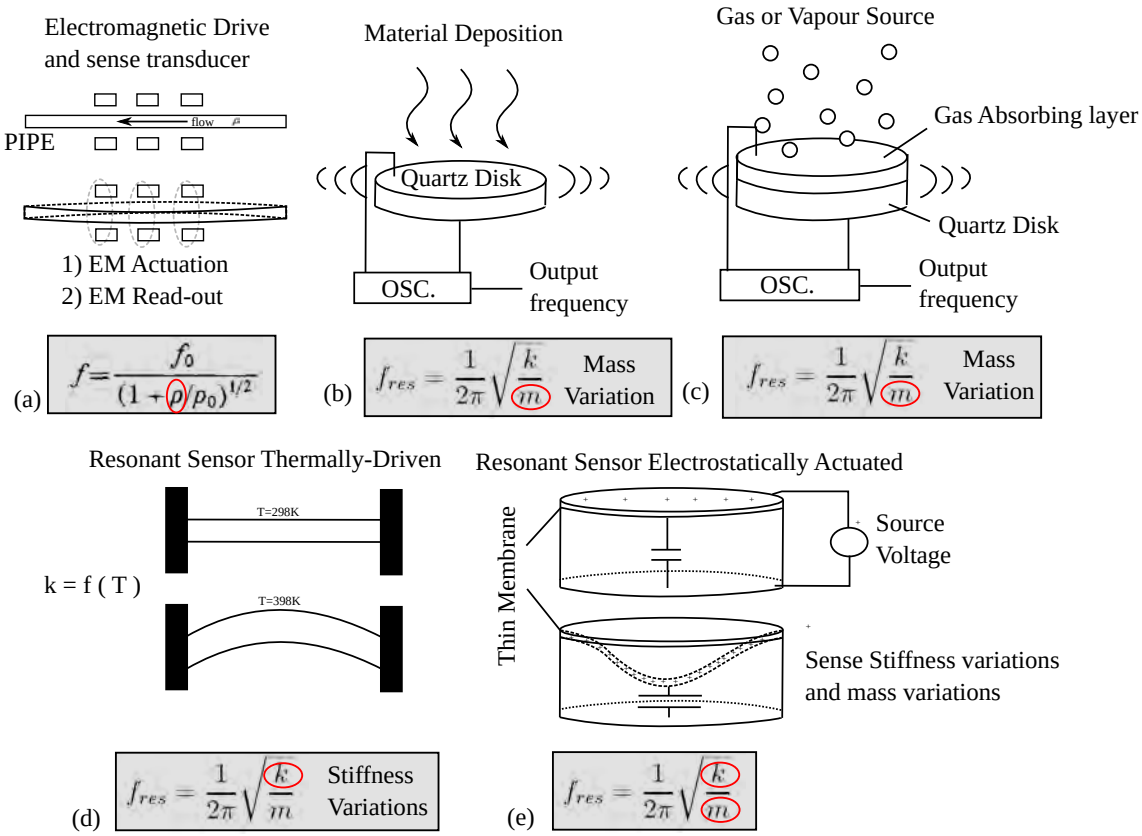

Figure 2.2: Examples of Resonating Sensors. [1]. (a)Fluid density sensor. (b) Mass sensor. (c) Gas Detector. (d) Thermometer. (e) Electrostatic sensor.

transducer can be used to force the pipe into vibration, then the electromagnetic coupling of the same sensor can be used again to read-out the resonant frequency of the pipe. Fig.2.2(b) shows a quartz resonator, which can be used to monitor material deposition during a generic fabrication process. Same principle can be used to detect gases in a local environment as shown in Fig.2.2(c). Fig.2.2(d) shows how the transducer thermal expansion can be used to modify its stiffness and resonant frequency to monitor the surrounding temperature. Fig.2.2(e) shows a sensors which is electro-statically actuated. A voltage source is used to bend a membrane and then released to vibrate at its natural oscillation mode. The frequency of vibration of this thin membrane depends on the mass and the stiffness of it. In more advanced and complex systems, MEMS sensors are preferred. These devices are based on the same transducing principle of the discrete sensors. However, the design of these transducers require particular attention to issues, which don't need to be taken into account in the discrete sensor design and fabrication. In order to overcome these

issues some of these MEMS are designed into exotic shapes shown in Fig.2.3.

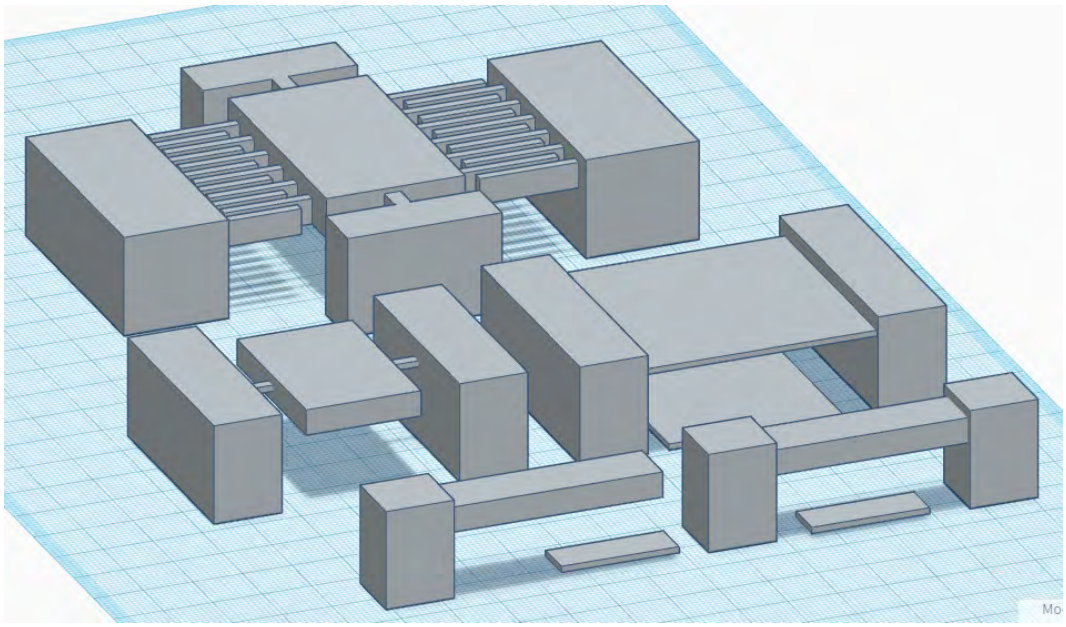

Figure 2.3: Examples of MEMS Resonating Sensors Structures.

Regardless the complexity that they presents, they can be seen as composed by basic structures, which are easier to study, such as cantilevers, bridges and membranes. This alternative interpretation can simplify the analysis of the whole transducer. These sensors can introduce a certain kind of noise related to their geometrical dimensions. This is usually labelled as high order oscillating modes. There are many high order modes, each one of them represents a different way to vibrate of the transducer. Each mode is characterized by a particular frequency and it can be activated only if the exciting signal provides enough energy at that frequency. Therefore, the oscillating mode at which the structure is vibrating depend on how the excitation distributes the energy along its frequency spectrum. Examples of high order modes are simple to visualize for the case of a cantilever as shown in Fig.2.4. Fig.2.4 shows also possible vibrations shape in other structures.

2.3 Modelling of a Resonating Sensor

An electrical model of a resonant transducer is essential to understand the interactions with the electronic interface used to read-it out. As shown in Fig.1.3, the resonating transducer is modelled generally as a two port device however, under

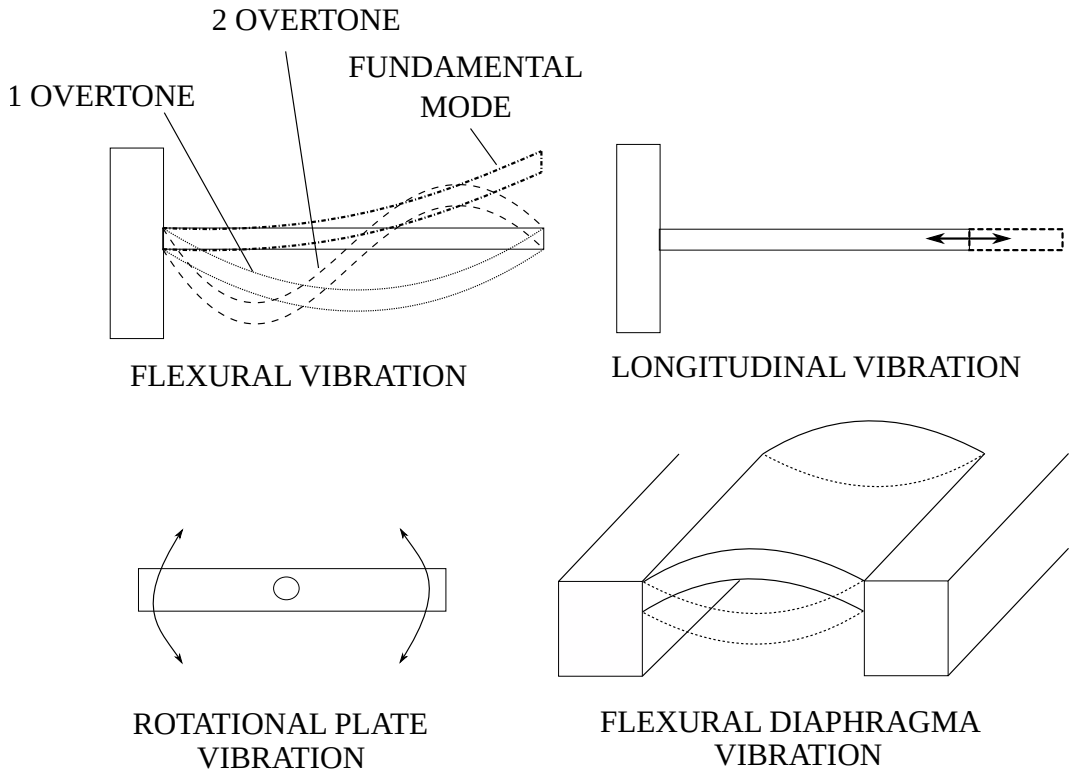

Figure 2.4: Example of vibrations in resonating sensors.

particular assumptions it can be approximated with a simple resonant bipole. The simple way to investigate an equivalent model for this type of transducer, consists in analyzing its electrical impedance. By using an impedance analyzer it is possible to observe that this type of device present a frequency behaviour similar to a second order linear system, which can be approximated with a RLC circuit. An example of resonant transducer impedance plot is shown in Fig.2.5(a).

Fig.2.5(a) shows multiple peaks, but analyzing just the first one it is possible to find some similarities with a second order linear system as shown in Fig.2.5(b). Overlapping these two curves it can be observed that they match till the point at which the impedance reach the minimum value, while in the second part of the plot the two curves show different behaviours (Fig.2.5(b) black line and red dashed line). This means that a RLC circuit can model a resonant sensor with a quite good approximation at the resonance, after that the simplified model starts to introduce a certain error. A better approximation can be obtained by adding a parallel capacitance to the RLC series circuit. This new model is often referred to as Butterworth Van Dike model (BvD), where this new element is actually representing the parasitic

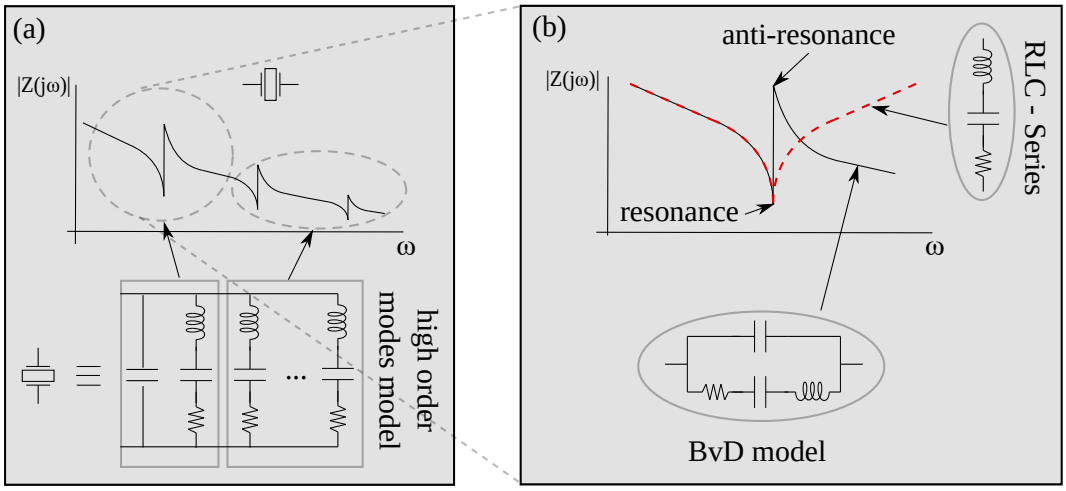

Figure 2.5: Resonating Sensor models. (a) Example of a real resonating sensor impedance plot and equivalent model. (b) Comparison of the RLC and BvD impedances with the impedance of a resonating transducer around the fundamental mode.

capacitance between the electrodes of the transducer. The parasitic capacitance in the BvD model introduces the anti-resonance peak and the continuous decreasing of the impedance, which otherwise should increase due to the effect of the inductance as it occurs for the RLC impedance plot. In some cases, the effects of this capacitor can be neglected such as in electromagnetic transducers in which a simple RLC series circuit provides enough accuracy to model the behaviour of the resonating sensor. In other cases such as in electrostatic and piezoelectric transducer the parasitic capacitance of the electrodes cannot be neglected. The previous observation are limited to the range around the first peak in the impedance plot, which is also referred as fundamental mode or fundamental frequency. The previous model don't take into account the other peaks in the impedance plot in Fig.2.5(a). These peaks represent the higher order modes and each one can be modelled by a single RLC series.

Therefore, if these modes are not negligible an improved model consists in additional RLC series circuit connected as shown in Fig.2.5(a). The research about the modelling of this device brought out many other models, which improve the accuracy of the approximation done, some of these are: the Guan model [22] and the transmission line model based on the Mason model [23] as shown in Fig.2.6. The

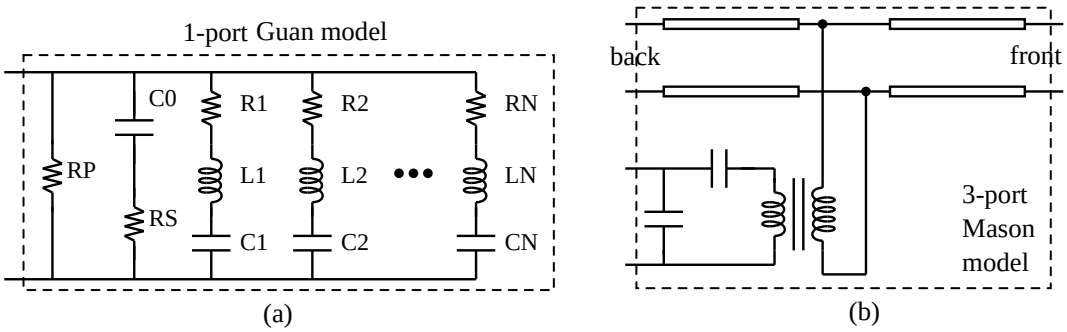

Figure 2.6: Other models for resonating sensors. (a) Guan Model (b) Transmission Line model based on Mason model.

Guan model is often used when a description of the higher order modes and losses in the resonant sensor are needed. While the transmission line model is utilized to model piezoelectric transducer, emphasizing the energy transfer at the surface interface of the transducer. It is a 3 port model, where one is the electrical port and the other two are the mechanical ports, which are often referred as back acoustic port and the front acoustic port. For instance, given a piezoelectric disk the two ports represent the propagation of the energy through the two opposite surface of the disk. In conclusion, the choice of the correct model depends just on the accuracy required.

Chapter 3

Bidirectional Amplifier

The bidirectional Front-End developed in this work is based on a pseudo floating gate structure. Therefore, this chapter concentrates on analysis and design of this electronic circuit and explains the basic idea of how to transform this unidirectional amplifier into a bidirectional device.

3.1 Pseudo Floating Gate Amplifier (PFGA)

Operational amplifiers (OP-AMP) have been used intensively in analog electronic circuit design such as in filter design, switched capacitor circuits [24], low noise amplifier (LNA) [25], sensor front-end [26] etc. However, the demands for low power and down-scaling of the micro-electronic systems introduces new challenges in the architecture of this type of device. One of the many issues, is the design of low power OP-AMPs for low supply voltages [27] specially for analog applications.

The typical structure of an OP-AMP requires minimum 3 stacked devices as shown in Fig.3.1(a), which limits the minimum power supply of this circuit. Furthermore, all the high gain OP-AMPs based on cascode stages are not suitable building blocks to implement low power amplifiers, because their high number of stacked MOSFETs doesn't allow reducing the power supply voltage (Fig.3.1(b)). Therefore, novel solutions have been developed. Some still based on the OP-AMP structure, but without the current tail, which reduces the number of stacked devices to two [28] as shown in Fig.3.1(c). Other researches proposed solutions based on the use of the logic inverter for analog applications (Fig.3.1(d)). An alternative solution

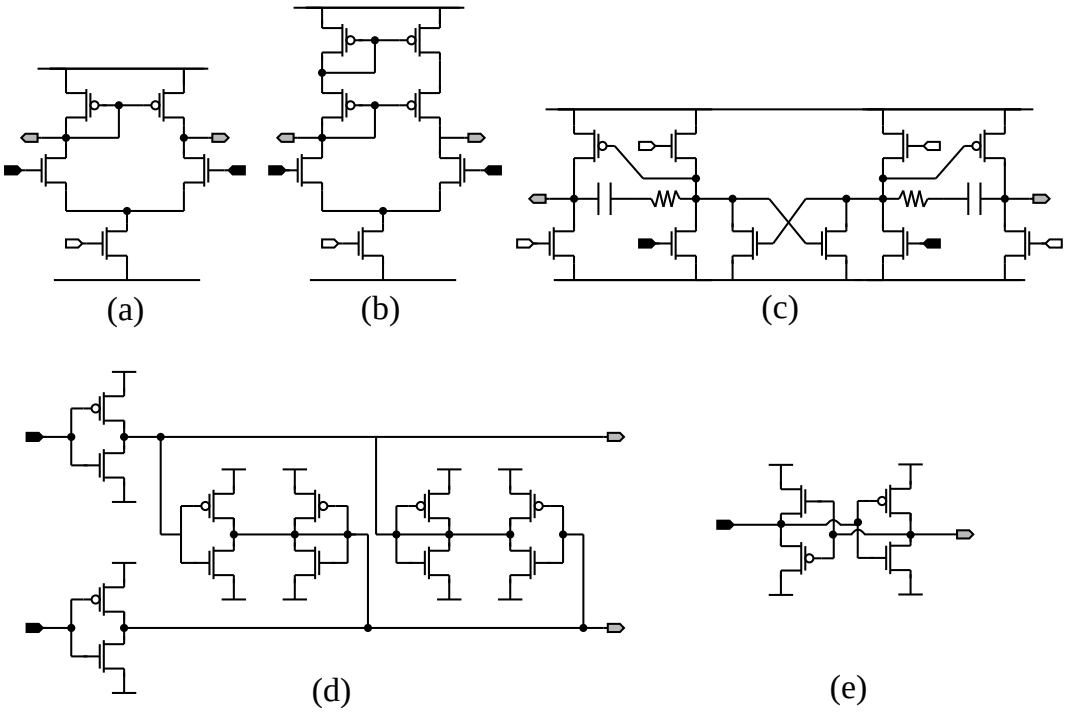

Figure 3.1: OP-AMP amplifiers State of the Art. Black Terminals are the input of the amplifiers and the grey terminals are the output terminals. (a) Typical differential input stage for OP-AMP based on 3 stacked transistors. (b) Cascode input stage of OP-AMP. (c) OTA without tail current. (d) Inverter Based OTA. (e) Pseudo Floating Gate Amplifier (PFGA)

proposed and studied in the last two decades is called Pseudo-Floating Gate Amplifier (PFGA) shown in Fig.3.1(e). This type of device enjoys the advantage of using an inverter-based amplifier with only 2 stacked transistors and is based on the floating gate transistors. This new structure allows a very low power supply and an easy implementation in CMOS technology. This new type of amplifier has been proved to be effective and it has been utilized to implement many type of circuits such as for multivalued gate (MV) [29], analog to digital converters [30], band pass filters [31, 32, 33, 34], tunable filters controlled with bulk voltages [2], tunable dual-band pass filters [35], filters based on current-starved PFGA [36, 37], re-configurable analog circuits [38], to implement mixer and extractor [39],multiplexer/demultiplexer [40]. Some of the electronic circuits implemented with PFGA, which can be used as building blocks to realize more complex analog systems are shown in Fig.3.2.

The flexibility of the PFGA is one of the main key points, which makes this

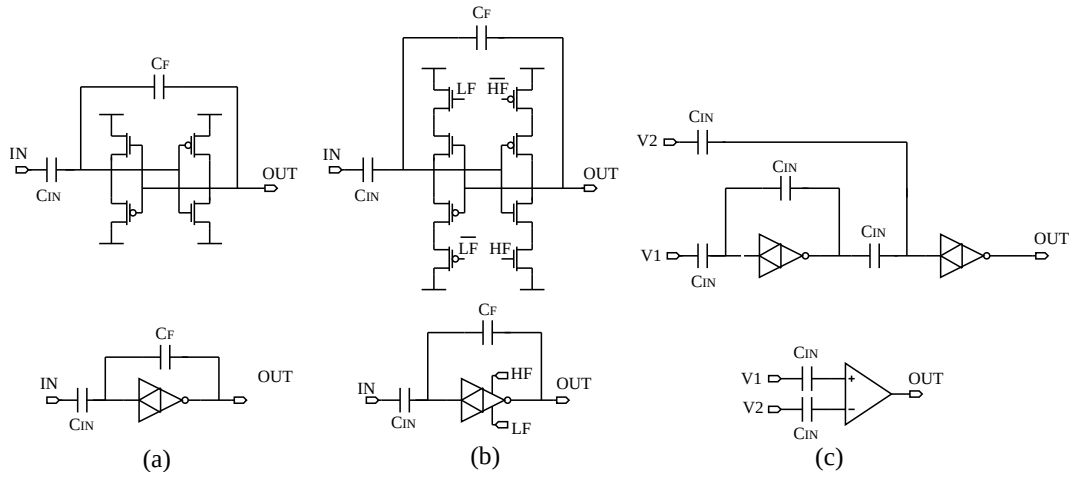

Figure 3.2: Basic building blocks implemented with PFGA. (a) Inverting Amplifier. (b) Bandwidth controlled Amplifier (c) Operational Trans-conductance Amplifier (OTA).

amplifier very suitable for all type of applications. Furthermore, the possibility to implement bidirectional systems by using this device has been introduced in [38], [13], [39], [34],[41],[40]. This idea is the basic concept, which led the author to conduct a research on the bidirectionality of the PFGA and its applicability as bidirectional front-end for resonating sensors.

3.2 PFGA Basic Principle

This section will describe the structure and the working principle of the PFGA shown in Fig.3.3.

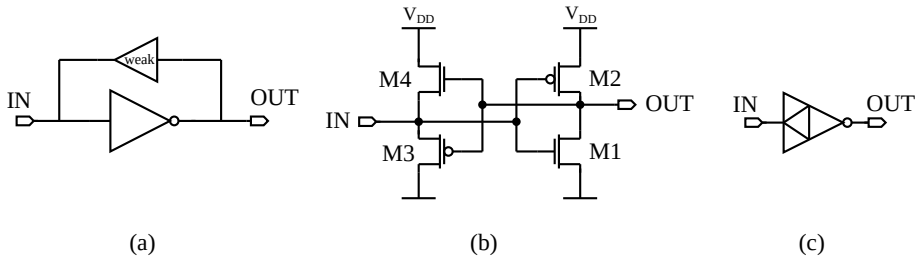

Figure 3.3: Pseudo-Floating Gate Amplifier. (a) System Level. (b) Transistor Level. (c) Symbol for the PFGA [2]

The PFGA is based on a CMOS inverter closed in a feedback loop with an ideal voltage buffer as shown in Fig. 3.3(a). Fig. 3.3(b) shows a PFGA made by

only 4 MOSFETs. $M1, M2$ realize a CMOS logic inverter, while $M3, M4$ realize a CMOS voltage buffer. The symbol adopted in literature to represent this amplifier is shown in Fig. 3.3(c). The voltage buffer provides the biasing for the inverter, which is forced to work in linear region as amplifier rather than a logic device. By using capacitors it is possible to build a second feedback loop to set the gain of the PFGA. The gain is equal to $-\frac{C_{IN}}{C_F}$ in Fig. 3.2(a). The equilibrium state of the PFGA is characterized by $V_{IN} = V_{OUT} = V_{DD}/2$ when it is implemented by using a balanced inverter ($\frac{(W/L)_n}{(W/L)_p} = \frac{k_p}{k_n}$). This value can be graphically represented as the point at the intersection between the VTC curve of an inverter and the VTC curve of the voltage buffer as shown in Fig. 3.4. One of the peculiarity of this circuit is that the feedback reaction is provided by leakage currents of the MOSFET in the CMOS voltage buffer.

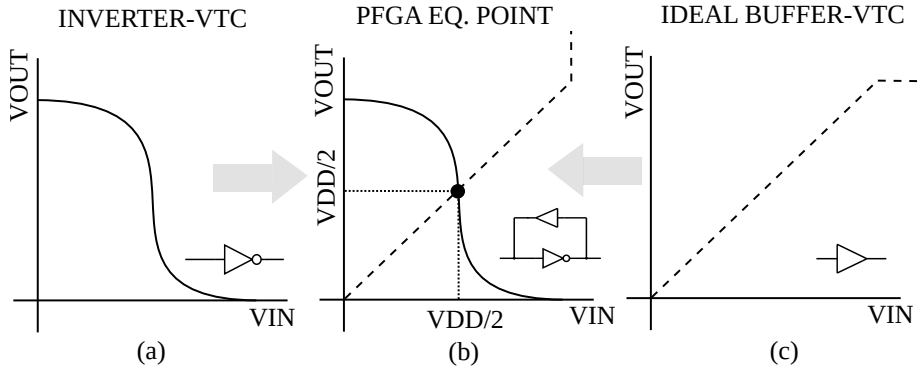

Figure 3.4: Pseudo-Floating Gate Amplifier Graphical Representation of the Equilibrium Point. (a) Inverter voltage transfer characteristic. (b)PFGA equilibrium point graphical representation. (c) Ideal Voltage Buffer voltage transfer characteristic.

For short channel transistors, these leakages provide enough current to charge and discharge the input node of the PFGA. It is important to emphasize that previous works about PFGA considered the sub-threshold currents as the dominant contribution to the leakage currents in the voltage buffer of the PFGA. This is an important assumption since in the new CMOS processes other sources of leakages could be dominant. A graphical representation of the feedback reaction in PFGA is shown in Fig.3.5. Fig.3.5(b) and (c) show that one of the MOSFET in the voltage buffer start to generate a current to bring back the equilibrium in the PFGA,

which is initially imbalanced. This process ends when $V_{IN} = V_{OUT} = V_{DD}/2$. In Fig.3.5(b) is the NMOS in the voltage buffer which drives the feedback reaction, while in Fig.3.5(c) is driven by the PMOS.

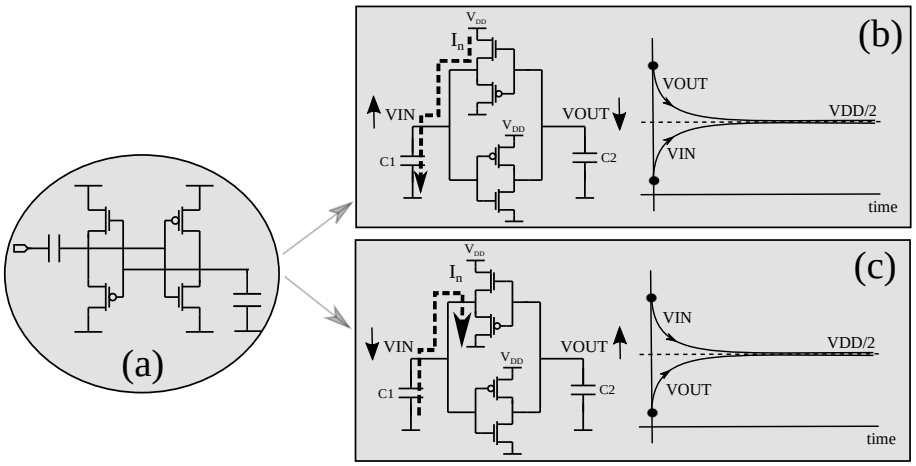

Figure 3.5: Pseudo Floating gate feedback reaction principle. (a) PFGA. (b) PFGA with initial condition $V_{IN} < V_{DD}/2 < V_{OUT}$. (c)PFGA with initial condition $V_{IN} > V_{DD}/2 > V_{OUT}$.

3.3 Effects of Channel Leakages in PFGA

The design of the bidirectional amplifier treated in this work requires a deep understanding of the PFGA operations. Therefore a detailed analysis of the PFGA has been described in [19]. However, the performance of the PFGA are strictly related to the value of the leakage currents used to bias it. Therefore, they must be distinguished in two cases, when the PFGA is implemented in high leakage CMOS technology, and the case where the PFGA is implemented in low leakage CMOS technology. The first one corresponds to the case of an implementation by using modern fabrication processes and it can find easy application in low voltage electronic circuits. The second one can be utilized in high voltage applications ($V_{DD} > 5V$) where low leakage technologies are the only option. Typically, the magnitude of the MOSFET leakages decreases as the dimensions of the transistor increase. Therefore, low leakage PFGA can be implemented by using old fabrication processes or power MOSFET. In literature, it has already been discussed a high leakage implementation in 90nm CMOS process, while this research focuses on the analysis of a

low leakage implementation and a comparison between these two technologies. The main difference between these two implementations is the time needed to approach to the steady state as shown in Fig.3.6.

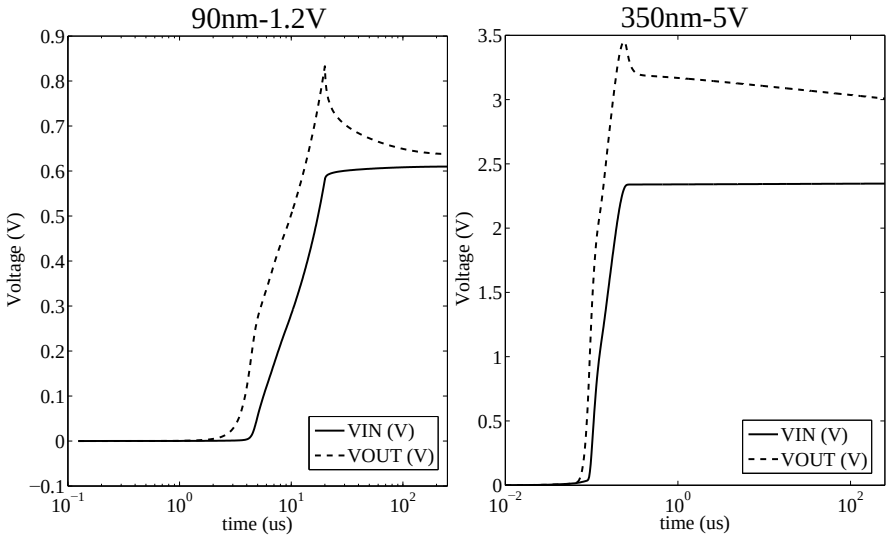

Figure 3.6: Initial transient time comparison between HL-PFGA (PTM-90nm) and LL-PFGA (AMS-350nm).

Fig.3.6 shows a comparison between an initial transient time of a 90nm and a 350nm implementation. The 90nm PFGA reaches the equilibrium state after a short initial transient time, while the 350nm PFGA will require longer time. This is due to the fact that in the high leakage PFGA (HL-PFGA) the feedback reaction is led by sub-threshold currents when the voltage buffer turns off. unfortunately, these currents are too low to drive the feedback reaction also in a low leakage PFGA (LL-PFGA). Therefore, the bias point of the LL-PFGA stops when the voltage buffer turns off. This problem has been discussed in [19], and it must be solved in order to obtain a functional amplifier. This issue is referred in this work to as offset of the PFGA, because the improper position of the bias point could be though as originated by an input offset voltage.

An interesting feature of the PFGA which does not dependent on the technology used to implement it, is the non linearity around the low cut-off frequency. This phenomenon is caused by the voltage buffer, which is driven by a wide input signal that emphasize the non linear relation between the input voltage and the output current of this device. The distortion of the signals in this amplifier can be quantified

by using the parameter called total harmonic distortion (THD). This non linear behaviour has been exploited for a low leakage PFGA in [19] and shown in Fig.3.7, but similar results can be obtained for an high leakage implementation.

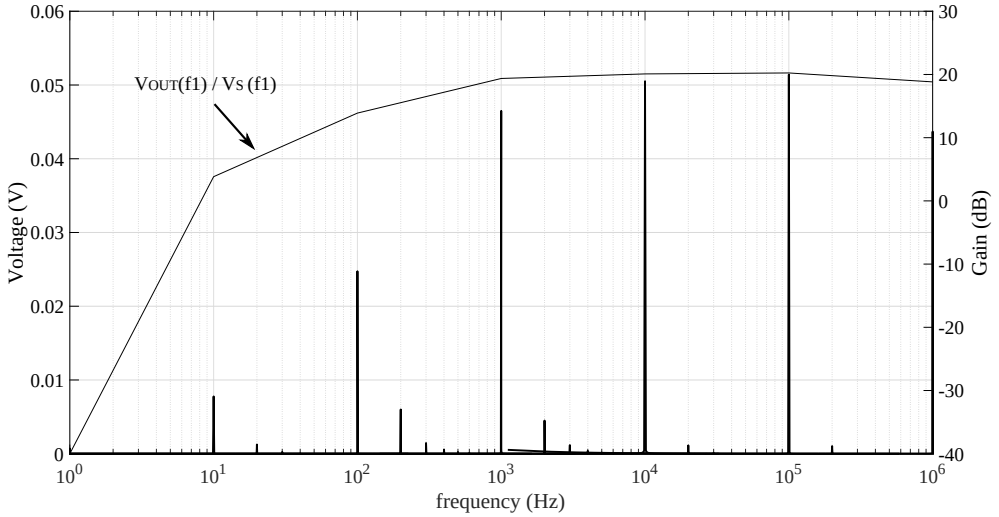

Figure 3.7: Non linear behaviour of the LL-PFGA around the low cut-off frequency.

Given the distortion introduced by the PFGA, it is not possible to use the ratio between the input and the output signal amplitude to evaluate the transfer function of the amplifier. The transfer function of the PFGA has been calculated by using the ratio between the input signal and the first harmonic of the output signal of the PFGA. Simulation and measurement results show that the non linearities are very low for a LL-PFGA but they are expected greater effects in a HL-PFGA. Indeed, a comparison between the AC analysis by using PTM-90nm model and the transfer function calculated considering the only first harmonic of the output signal, proved that the there exists a difference in the estimation of the low cut-off frequency. These results are shown in Fig.3.8. This is because, SPICE substitutes all the models with the small signal equivalent circuits, which in this case introduces an error because the input signal of the voltage buffer is not small.

Last remark is about the particular set up that must be used to perform the measurements on this amplifier. The working principle based on leakages requires instruments with very high input impedance and very low input current leakages. This purpose can be achieved by using a voltage buffer between the PFGA and the measurement tools. In conclusion, a detailed analysis of the PFGA implemented with high leakage CMOS technology has been developed to increase the under-

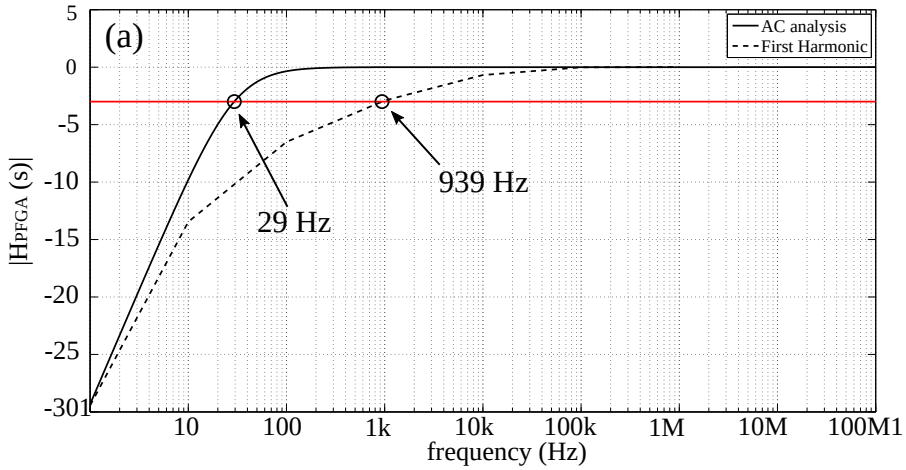

Figure 3.8: Non linear behaviour of the HL-PFGA around the low cut-off frequency.

standing of this device and define some precise design rules to minimize offset and non linearities.

Finally, [19] has been proposed a possible solution to solve the problem of the LL-PFGA offset. This task has been accomplished keeping the same structure and designing the inverter in the PFGA in order, which is not balanced anymore. Furthermore, a resistor has been added to improve the stability of the LL-PFGA bias point. Such PFGA has been proved to be a functional structure suitable to be applied for any high voltage application, specially as front-end for resonating sensors.

3.4 Bidirectional Pseudo Floating Gate Amplifier (BPFGA)

The bi-directionality of the PFGA has been exploited in a few previous works but only for low voltage applications [38], [13], [39], [34],[41],[40]. The working principle of a bidirectional PFGA is simple and represented in Fig.3.9.

The symmetry provided by the PFGA structure is used to achieve a bidirectional behaviour. The pair of MOSFET which implement a CMOS inverter, behaves as a CMOS voltage buffer when the power supply is swapped and vice-versa, a CMOS voltage buffer becomes a CMOS inverter when the power supply is reversed. This mechanism changes the orientation of the inverter inside the PFGA, which mimics

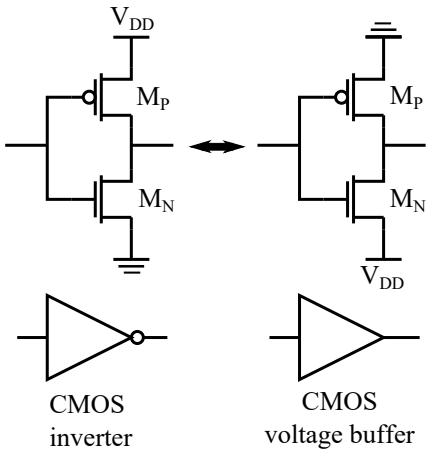

Figure 3.9: CMOS inverter and CMOS voltage buffer

the behaviour of a bidirectional amplifier. This circuit will be referred now on as Bidirectional Pseudo Floating Gate Amplifier (BPFGA). The basic idea is summarized and represented in Fig.3.10.

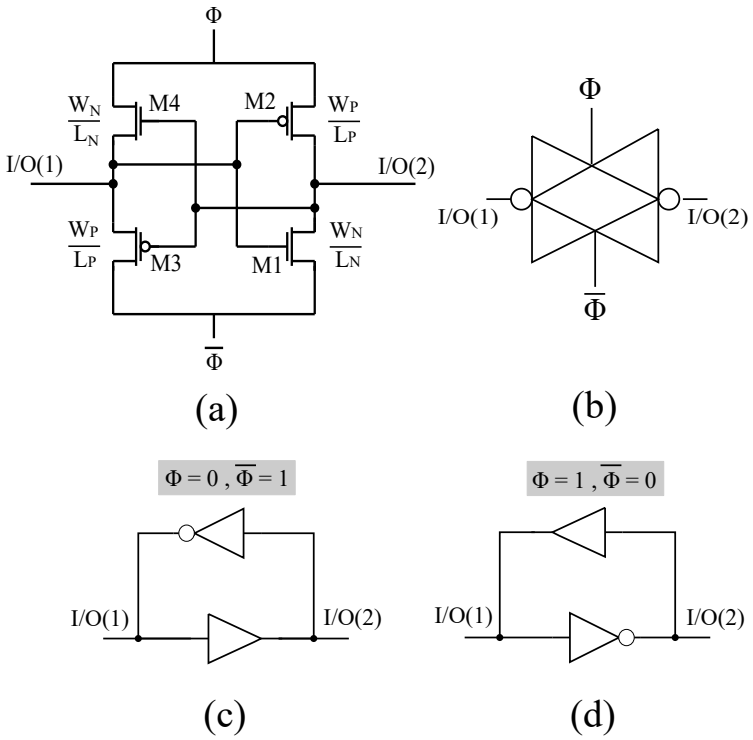

Figure 3.10: Bidirectional PFGA (BPFGA). (a) Transistor level implementation. (b) Symbol of the BPFGA. (c) and (d) show the elements in the BPFGA for the two possible cases.

The symbol chosen for the BPFGA is shown in Fig.3.10(b). The power supply of the BPFGA is now indicated with $\Phi, \overline{\Phi}$ since it is not anymore constant.

Fig.3.10(c),(d) report the cases already described. Two are the main parameters, which affect the BPFGA performances: the symmetry and the power supply. A PFGA is usually designed as asymmetric circuit (Fig.3.11(a)) and the buffer must be weakest possible. BPFGA should ideally have the same performances in both directions. This can be accomplished only if the BPFGA has a symmetric structure as shown in Fig.3.11(b). In this case, the aspect ratio of the MOSFET, which compose the inverter and the buffer are equals (Fig.3.11(d)).

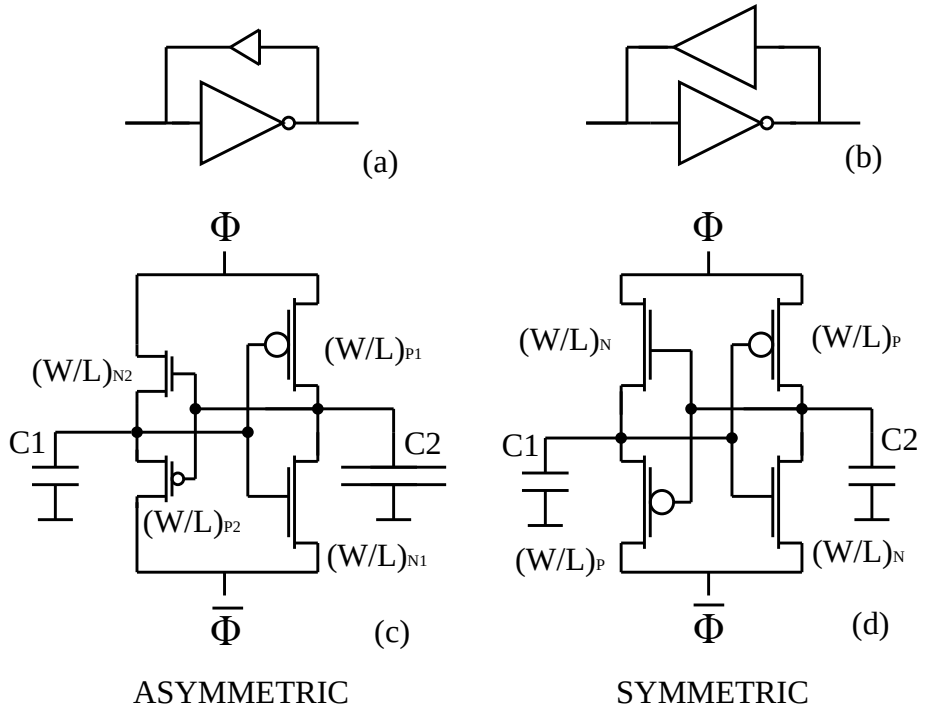

Figure 3.11: Comparison between symmetric and asymmetric design strategies. (a) Asymmetric PFGA. (b) Symmetric PFGA. (c) Asymmetric BPFGA. (d) Symmetric BPFGA.

The choice between an asymmetric and a symmetric structure depends on the value of the load at the two ports. When different loads are placed at the two ports of the BPFGA, an asymmetric structure is preferred as show in Fig.3.11(c), while when the loads at the two ports have similar values then a symmetrical structure is usually more convenient as shown in Fig.3.11(d). The second parameter to take into account during the design of the BPFGA is the technology utilized to implement it. For high leakage CMOS technologies (short channel MOSFET), the behaviour of the BPFGA can be considered almost ideal, which means that only the directionality of

the amplifier changes. However, when higher value of power supply are necessary ($\geq 5V$) then the BPFGA has to be implemented with older CMOS fabrication (low leakage CMOS technology) processes, which can support these voltages. In this last case the BPFGA is subjected to the problems previously described for the PFGA implemented in low leakage CMOS technology, such as high input offset voltage. These effects are discussed in detail in [19],[20]. A simple representation of the effects of the input offset is shown in Fig.3.12.

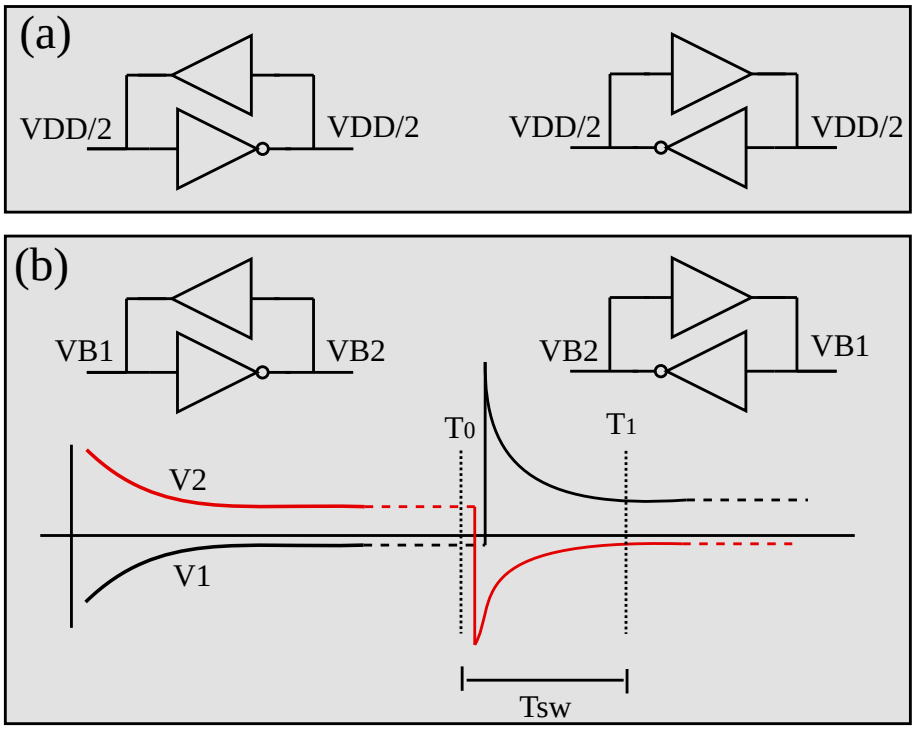

Figure 3.12: Dynamic analysis of the bias during the transition from a mode to the other one. (a) Equilibrium state dynamic in an ideal BPFGA. (b) Equilibrium state dynamic in real BPFGA. $T_1 - T_0$ is the time necessary for the bias point to reach the steady state values.

Fig.3.12(a) shows the ideal values for the input and the output node of the BPFGA before and after the transition from a mode to the other one. Fig.3.12(b) shows the working point dynamic for a low leakage BPFGA. When the system changes directionality ($t = T_0$), the bias voltages of the two nodes are ideally just exchanged. However, it can be noticed that the input voltage is the signal that will approach closer to the ideal value $V_{DD}/2$. This is due to the fact that the linear region of the inverter is usually very narrow and the input voltage can approach to

$V_{DD}/2$ before that the voltage buffer turns off and the dynamic of the bias point stops. t_{sw} is the time interval after which the bias point becomes almost constant.

Chapter 4

Bidirectional Front-End for Resonating Sensors

4.1 Bidirectional Front-End for MEMS Resonating Sensors

A bidirectional Front-End by using a BPFGA has been reported is shown in Fig.4.1.

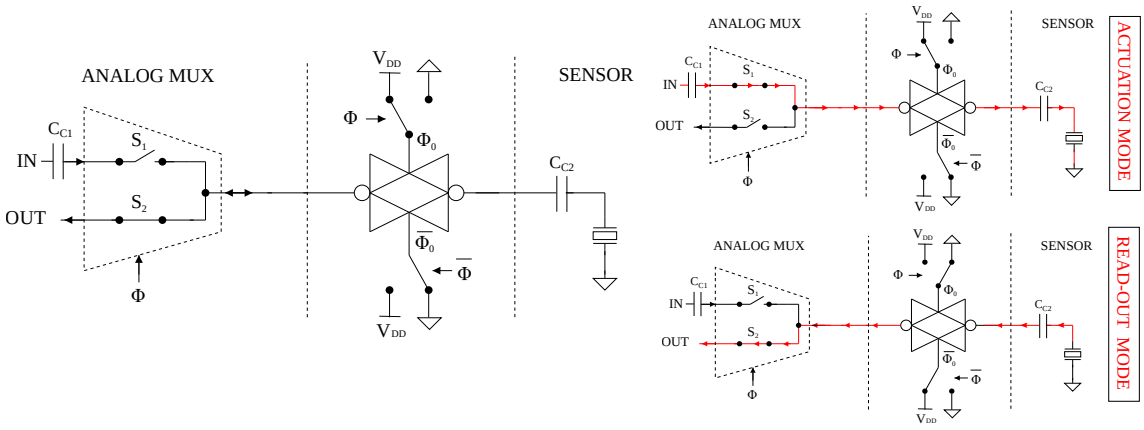

Figure 4.1: Bidirectional Front-End Working Principle.

The system is composed of a multiplexer/demultiplexer, 2 coupling capacitors, a BPFGA and a resonant load. The power supply of the PBFGA is controlled by two control signal Φ and its inverted form $\overline{\Phi}$. The working principle is divided in two phases: actuation phase and read out phase as shown in Fig.4.1. In the first mode the resonant sensor is excited by the electrical signal injected at the input

terminal of the Front-End. The input signal is a rectangular pulse characterized by a wide bandwidth spectrum that can force the load to resonate regardless the value of its resonant frequency. In read-out mode the electrical oscillation generated by the transducer is amplified by the BPFGA and read-out at the OUT terminal. The input terminal and the output terminal are connected to the BPFGA through 2 switches, which compose the multiplexer/demultiplexer. The concept has been proved in [13] by mean of simulations in 90nm Technology with a power supply of $1.2V$, which implement an high leakage BPFGA. The results are shown in Fig.4.2.

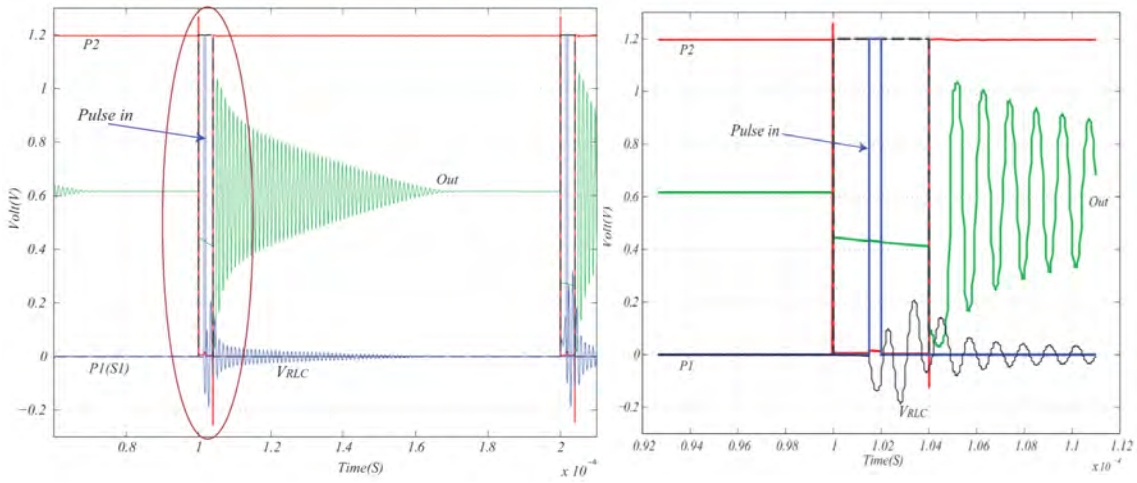

Figure 4.2: Simulation of the Bidirectional amplifier implemented in 90nm CMOS technology.

The resonant transducer behaviour has been reproduced by using a RLC series circuit. In order to mimic a variation of the resonant frequency, the RLC series has been implemented by using a variable inductor, which has been set to different values. Fig.4.2 shows that the input pulse (blue line) is injected while $\Phi = 1 = P1$ and $\overline{\Phi} = 0 = P2$. The sensor response V_{RLC} (black line) is an oscillating signal amplified by the PFGA during the read-out mode and read-out at the output terminal (green line). after being excited by the input pulse. The sensor response (black line) has been then amplified a read-it out at the output terminal (green line).

4.2 Measurement results of Bidirectional Front-End with RLC Load

This work proposes a deep study of the Front-End for resonating sensors with $V_{DD} \geq 5V$ using a CD4007 IC. This value has been chosen in order to provide signals with an amplitude easily to monitor with normal laboratory instrumentation and it allows to analyze the dynamic of the system, proving the functionality of the Front-End.

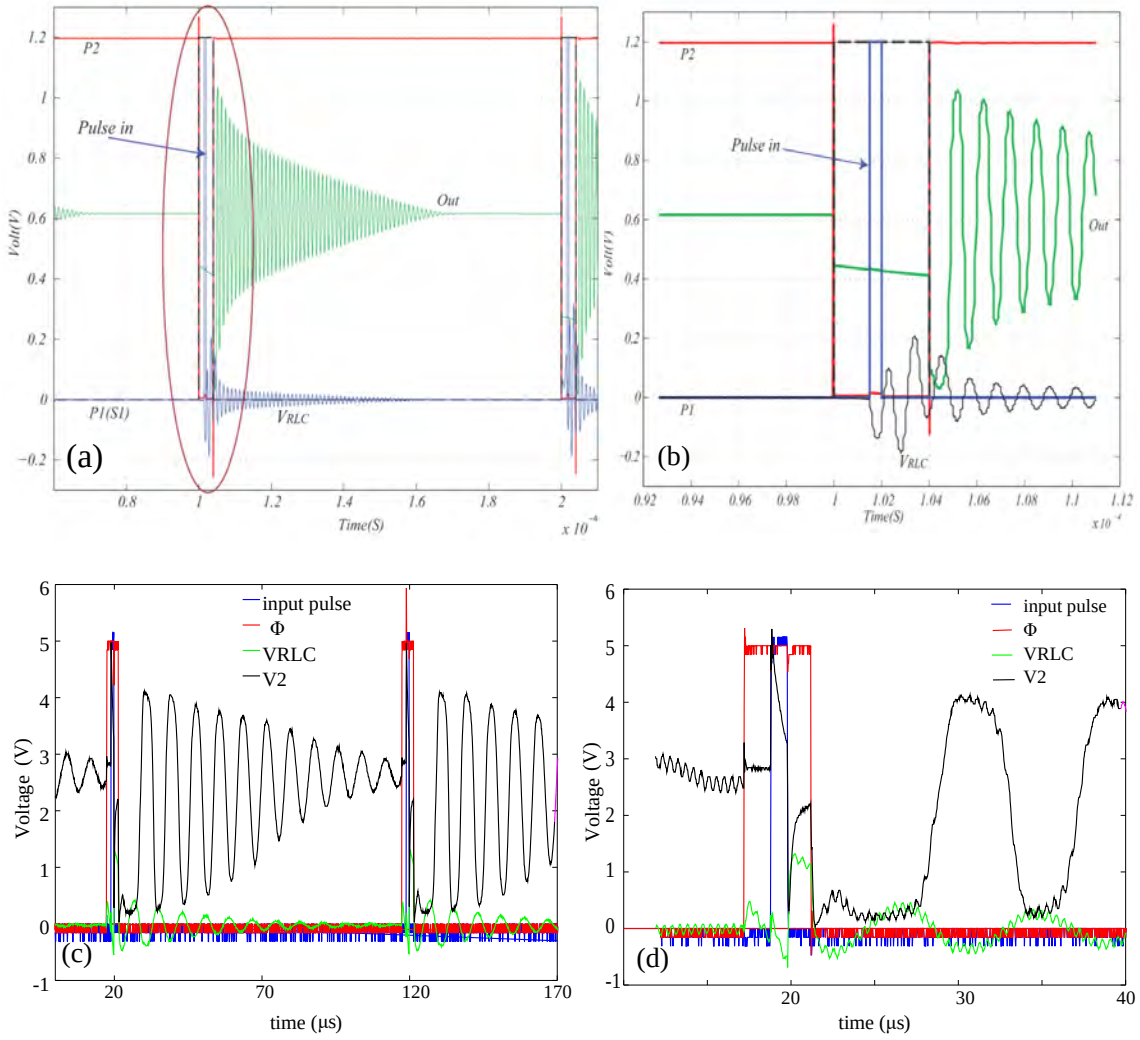

Figure 4.3: Comparison between the simulation results shown in Fig.4.2 and the measurements at $V_{DD} = 5V$. (a) Whole read-out cycle of the signals simulated with 90nm model. (b) Actuation mode analysis of the simulation results based on the 90nm model. (c) Whole read-out cycle of the signals measured on a prototype implemented by using CD4007UBE at $V_{DD} = 5V$. (d) Actuation mode analysis of the measurement results shown in (c).

Fig.4.3 shows the comparison between the measurement results of the bidirectional Front-End at $V_{DD} = 5V$ and the simulations shown in the previous section. Both tests have been performed by using an approximated RLC load which mimics the behaviour of a real sensor. Results do not show particular differences in the waveforms. A more detailed analysis of this Front-End revealed that this electronic circuit is subjected to secondary phenomena, which must be taken into account during the design. Some of these are represented in Fig.4.4

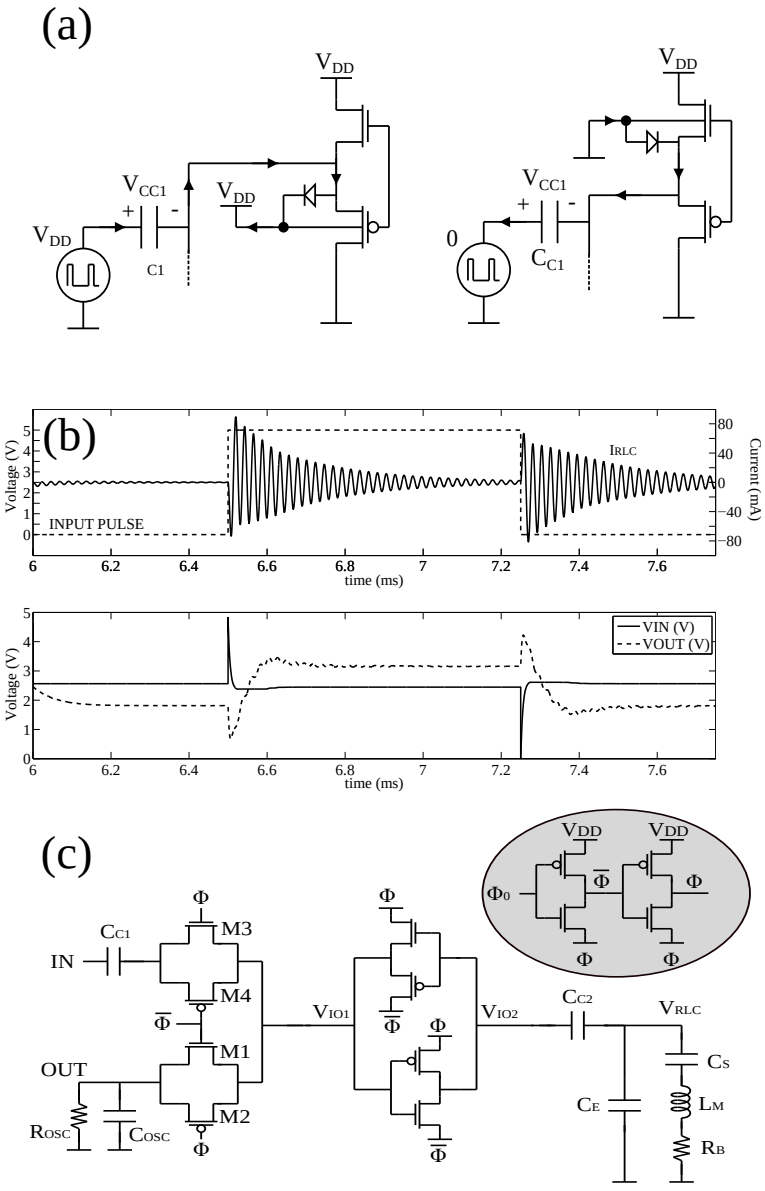

Figure 4.4: Secondary effects in the Bidirectional Front-End. (a) Turning on of the Source-Bulk pn junctions in the voltage buffer MOSFET (b) Double excitation of the resonant transducer. (c) Physical implementation of the Front-End.

First of all, at the occurrence of the edges of the input pulse the source-bulk pn junctions in the voltage buffer MOSFET could turn on as shown in Fig.4.4(b). This phenomenon increases the probability of latch up and the power dissipation of the circuit. Second, the sensor is excited by both edges of the input pulse which force the device to oscillate for two times. Third, the output swing of the amplifier is maximized only by implementing the multiplexer/demultiplexer with transmission gates as shown in Fig.4.4(c). A detail description of these and other phenomena is provided in [20]. In conclusion, the design of this Front-End consists mainly in fixing the values of the coupling capacitors and the parameter of the control signals to maximize the excitation of the sensor.

4.3 Bidirectional Front-End for Piezoelectric Sensors

The use of an approximated model for resonating sensors is very convenient from electrical point of view, because it allows the designer to test the electronic interface without the need of a real transducer. However,the accuracy provided by the approximated load must be verified. Therefore, a piezoelectric ceramic transducer has been characterized as shown in Fig.4.5 and utilized to test the bidirectional front-end.

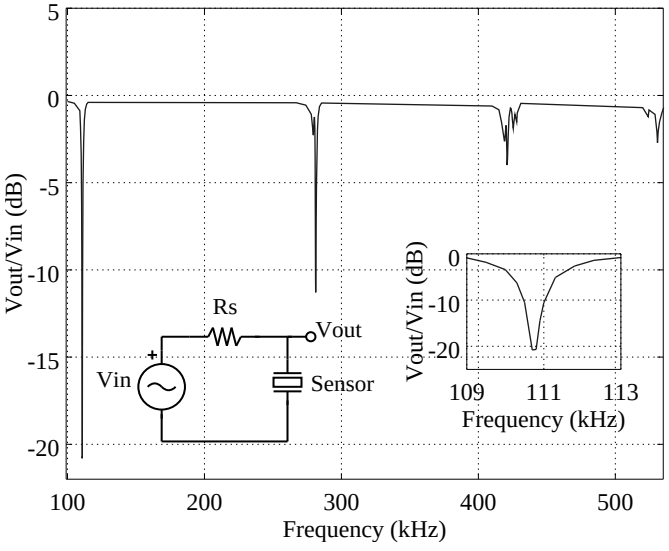

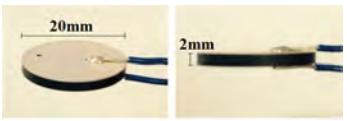

Parameters	Value
$R_b(\Omega)$	2.88
$L_m(mH)$	3.69
$C_s(pF)$	565
$C_o(nF)$	2.95

Figure 4.5: Piezoelectric Sensor Characterization

The detailed of the measurement set-up can be found in [15]. Measurement results have been compared in Fig.4.6 with those one shown in Fig.4.3 (c,d).

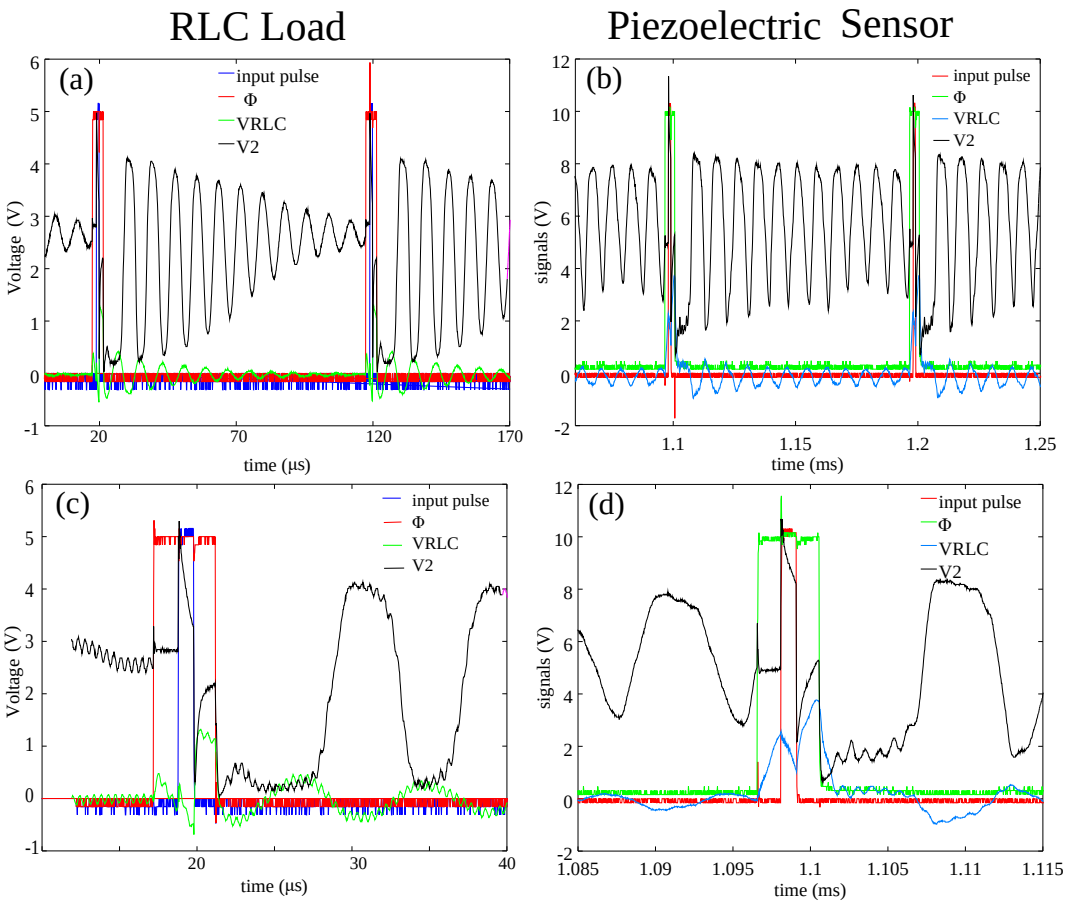

Figure 4.6: Comparison between the measurement results of the bidirectional front-end loaded by a piezoelectric sensor (a) vs RLC (b). Figures (c) and (d) are close-ups of (a) and (b) respectively.

A first analysis of Fig.4.6(a) and (b) shows very similar waveforms between the two cases. We have chosen two different power supply voltages to show that this parameter doesn't affect the shape of the waveforms. The excitation of a real transducer produces an oscillation which is less sinusoidal than the shape produced by the excitation of an RLC load. This is probably due to the non linearities of the transducer. The damping for the real piezoelectric sensor is much lower than the one observed with the RLC approximated model. This is due to the fact that $R_b = 100\Omega$ for the RLC load and $R_b = 2.88\Omega$ for the piezoelectric transducer. Fig.4.6(c),(d) highlight the shape of the wave-forms around the actuation mode. The main difference between the two cases is represented by the signal V_3, which is

characterized by fast variations in Fig.4.6(c) and slow variations in Fig.4.6(d) during the actuation mode. When the bidirectional amplifier drives the piezoelectric sensor, the dynamic of V_3 is slower because the presence of the parasitic capacitance C_E between the electrodes of the transducer. Furthermore, in both cases it is shown the presence of noise affecting the signals V_{RLC} and V_3, but they have different origins. When the RLC load is used, then the noise is probably due to the resonance of the inductor with some parasitic capacitance in the circuit, while when the real sensor loads the bidirectional amplifier, the noise is due to the higher oscillating modes. In conclusion, a comparison between the results in [14] and [15] shows similar results. This proves that the approximated load can be used in place of a real transducer and future tests can be performed without the necessity of a real device.

4.4 A Control System for a Low Power Bidirectional Front-End

One of the major concern, in the design of a portable device is the power consumption. In an analog electronic interface the most common and dominant source of power dissipation is due to the biasing of the amplifiers. In the BPFGA the major consumer of energy is the inverter, which is characterized by a constant current passing through the PMOS and the NMOS during the normal working operation. Therefore in [16] we proposed a simple control system to reduce the power consumption of the bidirectional Front-End. The idea behind this system is that the amplifier can be turned off after the measurement of a few periods of the output oscillating signal, which will provide sufficient accuracy to estimate the resonant frequency of the sensor as shown in Fig.4.7.

Ideally, one period of the oscillating signal would be even enough to obtain the required parameter, but due to the noise and other fluctuations in the signals of the Front-End the uncertainty of this parameter increases. In brief, the idea consists in introducing "sleeping mode" in the normal operation of the BPFGA. This design strategy can be easily implemented in this front-end because of the simple structure of the amplifier. This mechanism is shown in Fig.4.8.

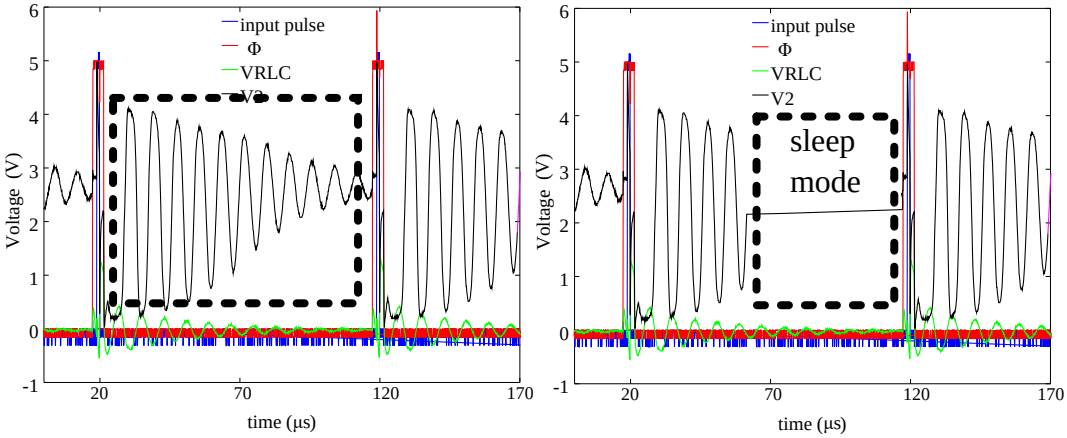

Figure 4.7: Sleeping Mode Concept

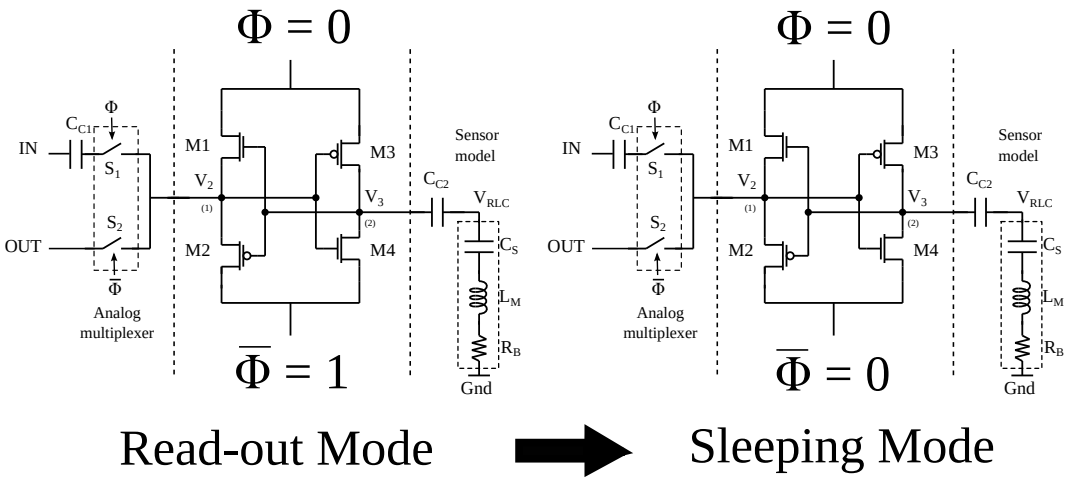

Figure 4.8: Sleeping Mode Implementation

Fig.4.8 shows that the amplifier can be turned off by imposing $\overline{\Phi} = 0$ during the read-out mode. The sleeping mode must be triggered by the occurrence of a certain number of periods of the oscillating output signal of the Front-End. The control system, which realizes the sleeping mode is shown in Fig.4.9.

This system counts the zero-crossing points at $V_{DD}/2$ of the output signal and after a certain number of periods turns off the power supply of the BPFGA. During the actuation mode the control system is bypassed by the AND gates U2 and U1. The whole system has been described in [16]. Finally, a comparison with the state of the art has been done to analyze the benefits provided by the sleeping mode and it is shown in Table 4.1.

This comparison shows that the BPFGA with sleeping mode reduces the power consumption to 16% of the power consumed without using this technique, which

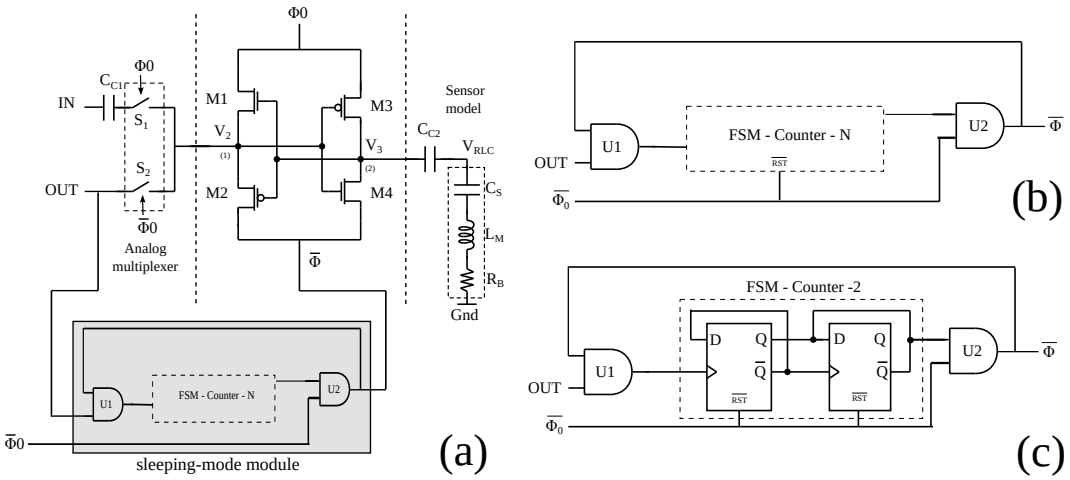

Figure 4.9: Sleeping Mode Control System. (a) BPFGA with generic sleeping mode module connected. (b) Generic Sleeping Mode module. (c) Sleeping mode control system triggered by one period of the output oscillation of the BPFGA.

Table 4.1: Performance comparison of resonating sensor front-end

Power diss.	**read-out method**	**Reference**
1.7 mW @ Vdd=5V	RDM wihtout sleep mode	current work
$270\mu W$ @ Vdd=5V	RDM + sleep mode	current work
$900\mu W$ to $1.95mW$ @ Vdd=5V	closed loop oscillator	[42]
$118\mu W$ @ Vdd=3.3V	RDM	[10]

corresponds to $270\mu W$. This value is comparable with the power consumption of the other structures described in literature, which means that this electronic interface shows competitive performance.

4.5 Bidirectional Front-End with Bandwidth Control

The flexibility of the proposed Front-End has been improved by introducing a simple way to control the bandwidth of the BPFGA. By adding only two transistors to the inverter/amplifier as shown in Fig.4.10(a), it is possible to control the output resistance of the amplifier and therefore the dominant pole as shown in Fig.4.10(b) and in Eq.4.1.

$$\omega_p = \frac{1}{R_{o-inv} C_L} \tag{4.1}$$

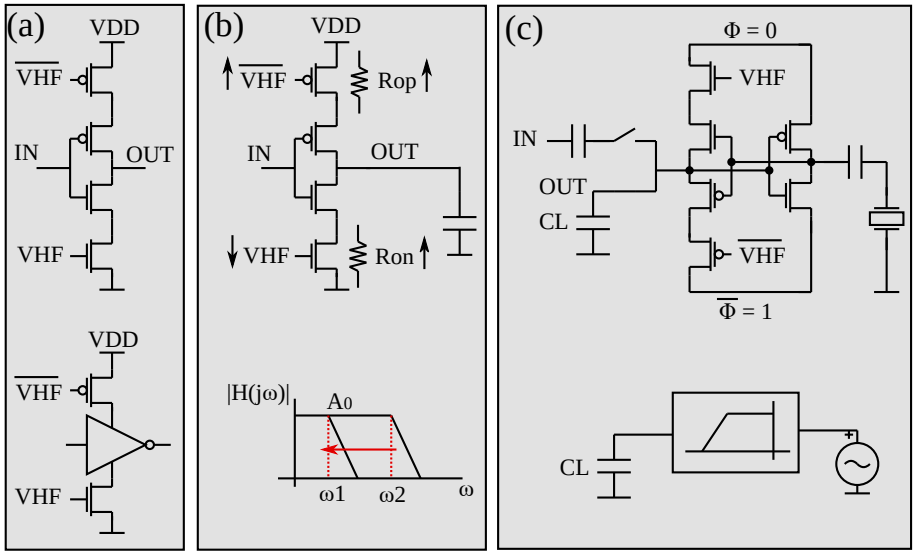

Figure 4.10: BPFGA with bandwidth control working principle. (a) Stacked inverter. (b) Bandwidth control concept. (c) Bidirectional Front-End with bandwidth control and equivalent model.

The stacked inverter shown in Fig.4.10(a) is controlled by two bias voltages: $V_{HF}, \overline{V_{HF}}$. If $|\frac{dR_{op}}{d\overline{V_{HF}}}| = |\frac{dR_{on}}{dV_{HF}}|$ then the relation between these two voltages is : $\overline{V_{HF}} = V_{DD} - V_{HF}$. Where: R_{on}, R_{op} are the drain source resistance of the NMOS and the PMOS controlled by the bias voltages. This new feature is particularly useful to remove high frequency noise over the output signal of the BPFGA, which for the case of a resonating sensor interface corresponds to the higher oscillating modes of the transducer (Fig.4.10(c)). Proved that the resonant transducer can be approximated with a BvD model, the electronic interface has been tested with this

equivalent load. The concept has been tested removing a sinusoidal signal generated by an auxiliar signal generator in series with the BvD model, which mimics an high resonating mode. The measurement results are shown in Fig.4.11.

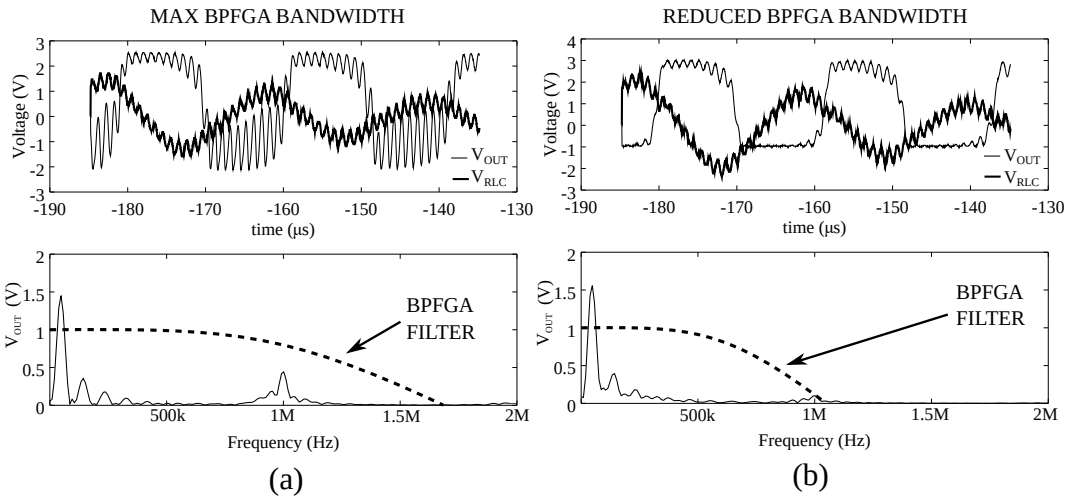

Figure 4.11: Effect of the bandwidth control on a high order mode oscillation at 1MHz. (a) Time and FFT analysis for the case of a high order oscillation inside the bandwidth of the bidirectional front-end. (b) Time and FFT analysis for the case of a high order mode filtered out by reducing the bandwidth of the amplifier.

The FFT analysis shows an attenuation of the "noise", which falls outside the bandwidth after the system has been tuned. Another benefit of reducing the bandwidth of the amplifier is the reduction of the amplifier power consumption, because the controlled MOSFET limit the current passing through the stacked inverter. More detailed about this structure can be found in [17].

4.6 An Auto-zeroing Bidirectional Amplifier for Resonating Sensors

The biasing network implemented by the CMOS voltage buffer has been proved to work well but it introduces also some design issues in terms of non linearities, power consumption and input offset. Therefore, in order to overcome all of these problems an alternative solution to implement an amplifier inverter-based has been investigated. The proposed Front-End is based on an unidirectional amplifier with

dynamic signal paths created by switches, which mimics the behaviour of a bidirectional amplifier [18]. The Front-End is represented in Fig.4.12.

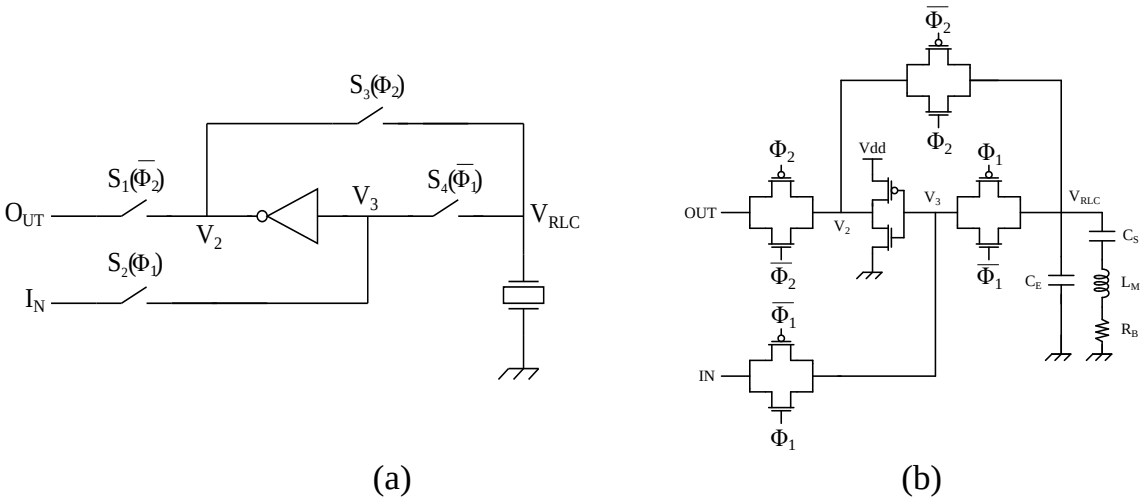

Figure 4.12: Auto-Zeroing Bidirectional Amplifier inverter-based (a) System Level. (b) Transistor Level.

The working principle is divided in three phases: actuation mode, auto-zeroing mode, read-out mode represented in Fig.4.13.

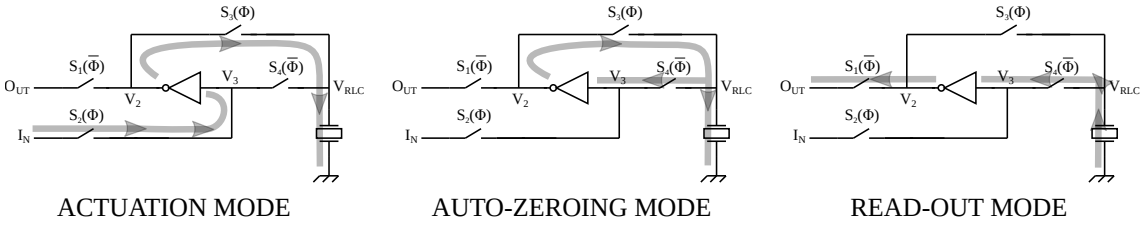

Figure 4.13: Working Principle Auto-Zeroing Bidirectional Amplifier

First of all, the sensor must be actuated, therefore switches S_2, S_3 close while S_1, S_4 remain open. A path from the input terminal to the sensor allows to excite the sensor. The second phase is called auto-zeroing phase and it is used to generate the bias voltage for the amplifier. The input and the output of the inverter are shorted in order that the voltage $V_M = V_{IN} = V_{OUT}$ is stored in the parasitic capacitance of the resonant transducer ($S_1 = S_2 = open, S_3 = S_4 = close$). Finally, the sensor must be read-out by closing the switch S_1 and opening S_3. In conclusion, the storage capacity of the transducer is used to keep the bias voltage across the sensor, which forces the inverter to work as amplifier. Since the most important phase in this

front-end is the storing phase of the bias voltage, this Front-End has been named as auto-zeroing amplifier.

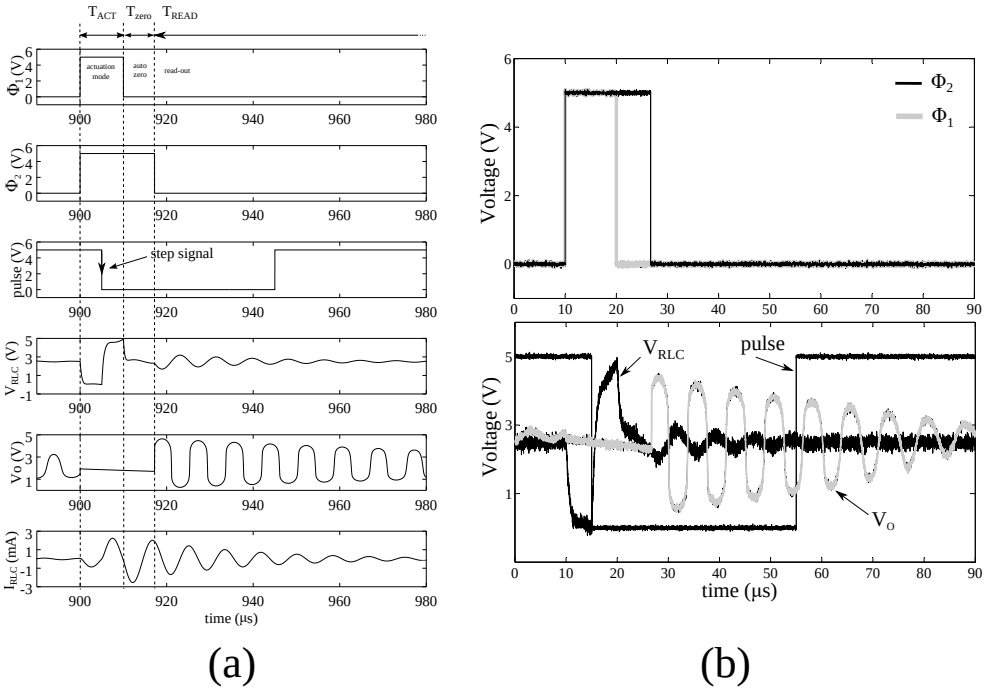

Figure 4.14: Comparison between Simulation Results (a) and Measurements (b) of the auto-zeroing amplifier.

Unfortunately, there two possible causes, which can affect the auto-zeroing phase, moving the bias point away from the ideal value. The first one is the charge injection due to the opening of the switch S_3. Second, the drop voltage on the output resistance of the inverter prevents the correct positioning of the amplifier bias point. All of these phenomena contribute to introduce an offset in the amplifier. By setting correctly the timing of the control signals and the parameter of the front-end it is possible to reproduce the same waveforms of the simulation results shown in Fig.4.14(a). A final comparison between the bidirectional amplifier based on BPFGA and the auto-zeroing amplifier inverter based, shows that the power dissipation of the biasing network is zero, while in the BPFGA is very small but not zero (leakage currents) and both structures present an input offset. On the other hand, the Auto-zeroing amplifier is an open loop amplifier, which means that is more affected to process voltage temperature variation (PVT) than the BPFGA.

Chapter 5

Conclusion and Proposal for Further Work

5.1 Overview

The Front-End described in this work is based on a Bidirectional Pseudo Floating Gate Amplifier. The bidirectional Front-End with all the added features is shown in Fig.5.1.

The same features are easily adaptable to the Auto-Zeroing bidirectional amplifier as shown in Fig.5.2.

Given its compact size and possibility of low power consumption, it can be used to drive even array of resonant discrete or MEMS transducers.

5.2 Conclusion

This thesis addressed the problem of designing an analog electronic Front-End for resonating sensors based on pseudo floating gate amplifier. One of the main contribution of this work consists in proving the functionality of this amplifier by measuring and testing on a real prototype. Design rules for these systems have been proposed based on a detailed analysis of the PFGA structure, which has been never reported before in literature. Additional features have been added to the basic Front-End structure to improve the performances and the flexibility of this electronic circuit.

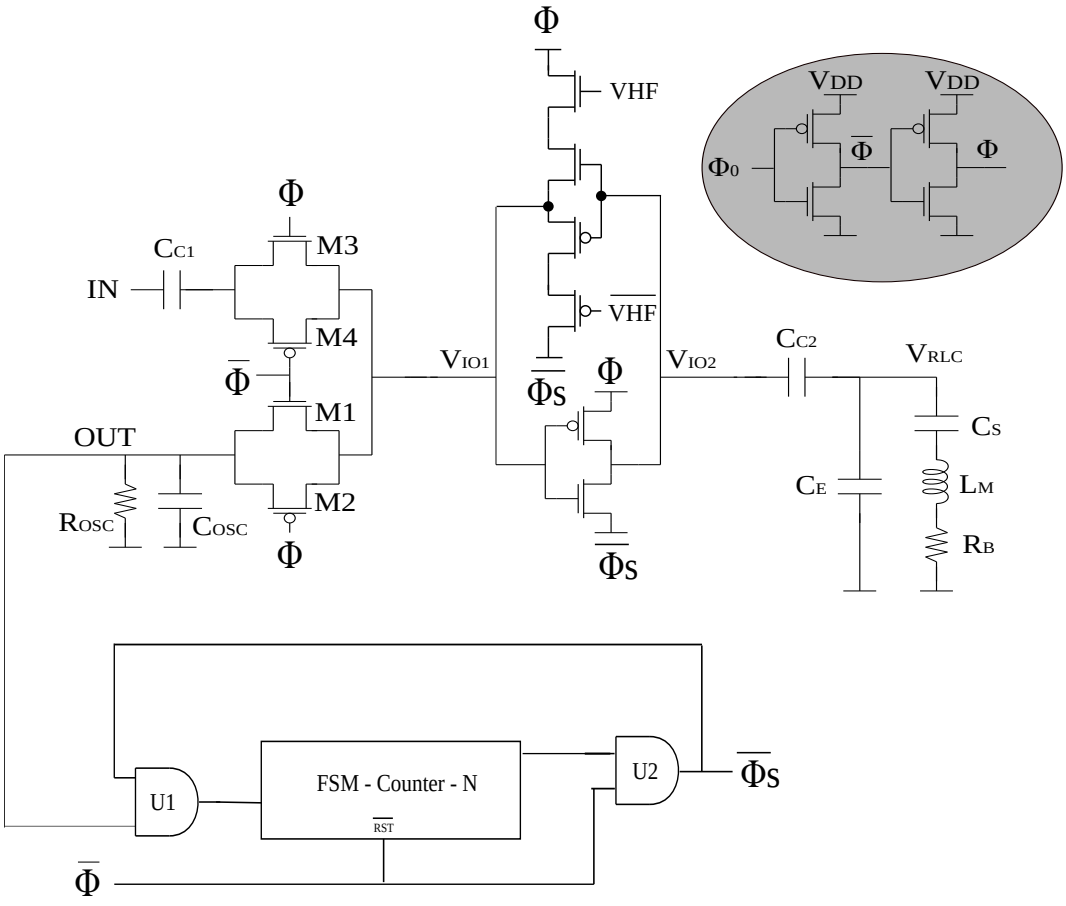

Figure 5.1: Whole BPFGA Front-End

A final comparison in terms of power dissipation has been done with the state of the art, which shows comparable performances with the other structure presented in literature.

5.3 Suggestions for Future Research

The next logical steps that should be taken are: implementation of the bidirectional Front-End in ASIC and test with a MEMS resonating sensor. The first one will improve the performance of the Front-End given the lower parasitic capacitance of the circuit and the possibility to perform and optimal design. The second one, will prove that the Front-End is suitable to drive a kind of device, which is the future trend for this type of sensor. Finally, a further step would be implement a MEMS and the ASIC in the same package to realize a whole system in one chip.

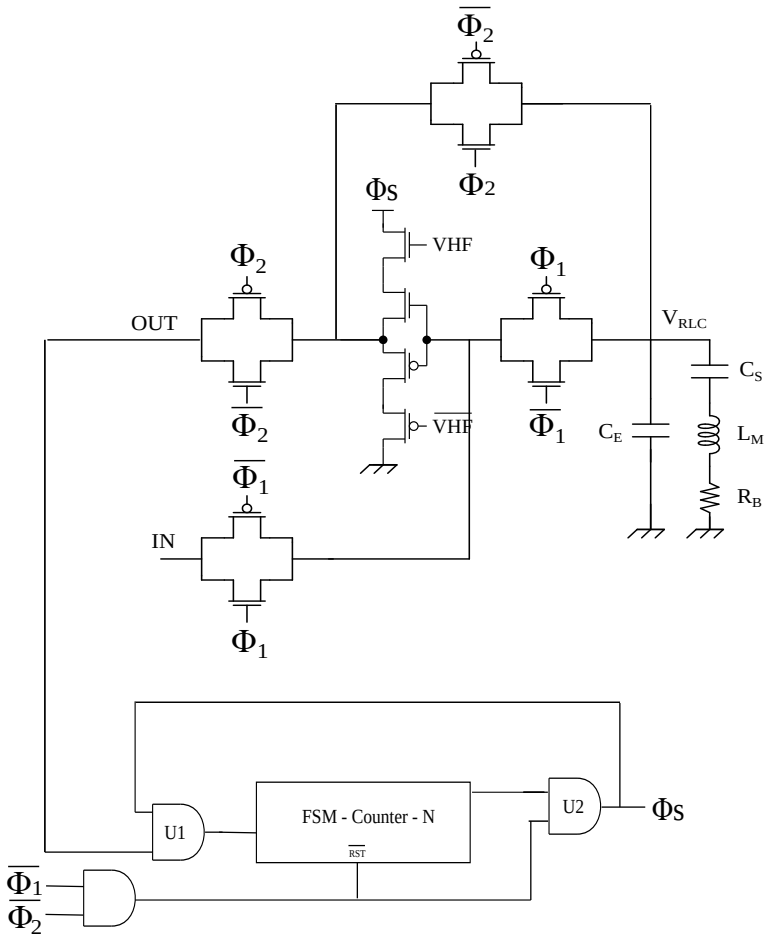

Figure 5.2: Whole switched Front-End

Bibliography

[1] R. M. Langdon, "Resonator sensors-a review," *Journal of Physics E: Scientific Instruments*, vol. 18, no. 2, p. 103, 1985. [Online]. Available: http://stacks.iop.org/0022-3735/18/i=2/a=002

[2] M. Azadmehr and Y. Berg, "An ultra-low voltage pseudo-floating gate amplifier," in *2012 IEEE Faible Tension Faible Consommation*, June 2012, pp. 1–4.

[3] J. K. Hart and K. Martinez, "Environmental sensor networks: A revolution in the earth system science?" *Earth-Science Reviews*, vol. 78, no. 3, pp. 177 – 191, 2006. [Online]. Available: http://www.sciencedirect.com/science/article/pii/S0012825206000511

[4] J. Edwards, "Signal processing drives a medical sensor revolution [special reports]," *IEEE Signal Processing Magazine*, vol. 32, no. 2, pp. 12–15, March 2015.

[5] W. J. Fleming, "Overview of automotive sensors," *IEEE Sensors Journal*, vol. 1, no. 4, pp. 296–308, Dec 2001.

[6] R. Bogue, "Mems sensors: past, present and future," *Sensor Review*, vol. 27, no. 1, pp. 7–13, 2007, https://doi.org/10.1108/02602280710729068.

[7] X. Zou and A. A. Seshia, "A high-resolution resonant mems accelerometer," in *2015 Transducers - 2015 18th International Conference on Solid-State Sensors, Actuators and Microsystems (TRANSDUCERS)*, June 2015, pp. 1247–1250.

[8] P. Parsons, A. Glendinning, and D. Angelidis, "Resonant sensors for high accuracy pressure measurement using silicon technology," in *Proceedings of the*

IEEE 1992 National Aerospace and Electronics Conference NAECON 1992, May 1992, pp. 349–355 vol.1.

[9] G. Stemme, "Resonant silicon sensors," *Journal of Micromechanics and Microengineering*, vol. 1, no. 2, p. 113, 1991. [Online]. Available: http://stacks.iop.org/0960-1317/1/i=2/a=004

[10] M. A. P. Pertijs, Z. Zeng, D. M. Karabacak, M. Crego-Calama, and S. H. Brongersma, "An energy-efficient interface for resonant sensors based on ring-down measurement," in *2012 IEEE International Symposium on Circuits and Systems*, May 2012, pp. 990–993.

[11] I. A. Ivan, M. Rakotondrabe, N. Chaillet, and P. Lutz, *Signal Measurement and Estimation Techniques for Micro and Nanotechnology*, 1st ed. Springer-Verlag New York, 2011, pp.29-69.

[12] J. Garnett E. Simmers, J. R. Hodgkins, D. D. Mascarenas, G. Park, and H. Sohn, "Improved piezoelectric self-sensing actuation," *Journal of Intelligent Material Systems and Structures*, vol. 15, no. 12, pp. 941–953, 2004. [Online]. Available: http://dx.doi.org/10.1177/1045389X04046308

[13] M. Azadmehr, B. K. Khajeh, and Y. Berg, "A bidirectional circuit for actuation and read-out of resonating sensors," in *2014 IEEE Faible Tension Faible Consommation*, May 2014, pp. 1–4.

[14] L. Marchetti, A. Romi, Y. Berg, O. Mirmotahari, and M. Azadmehr, "A discrete implementation of a bidirectional circuit for actuation and read-out of resonating sensors," in *2016 International Conference on Design and Technology of Integrated Systems in Nanoscale Era (DTIS)*, April 2016, pp. 1–5.

[15] L. Marchetti, Y. Berg, O. Mirmotahari, and M. Azadmehr, "Bidirectional front-end for piezoelectric resonator," in *2016 IEEE 13th International Conference on Networking, Sensing, and Control (ICNSC)*, April 2016, pp. 1–4.

[16] ——, "A control system for a low power bidirectional front-end for resonating sensors," in *2017 IEEE 14th International Conference on Networking, Sensing, and Control (ICNSC)*, May 2017.

[17] L. Marchetti, Y. Berg, and M. Azadmehr, "A bidirectional front-end with bandwidth control for actuation and read-out of mems resonating sensors," in *2017 24th International Conference on Mixed Design of Integrated Circuits and Systems*, May 2017.

[18] ——, "An autozeroing inverter based front-end for resonating sensors," in *2017 12th International Conference on Design Technology of Integrated Systems In Nanoscale Era (DTIS)*, April 2017, pp. 1–5.

[19] ——, "Analysis of the effect of channel leakage on design, characterization and modelling of a high voltage pseudo-floating gate sensor-front-end," *Electronics MDPI*, 2017, submitted.

[20] ——, "Design and modelling of a bidirectional front-end for resonating sensors based on pseudo floating gate amplifier." *Electronics MDPI*, 2017, submitted.

[21] T. Gast, "Sensors with oscillating elements," *Journal of Physics E: Scientific Instruments*, vol. 18, no. 9, p. 783, 1985. [Online]. Available: `http://stacks.iop.org/0022-3735/18/i=9/a=008`

[22] M. Guan and W.-H. Liao, "Studies on the circuit models of piezoelectric ceramics," in *International Conference on Information Acquisition, 2004. Proceedings.*, June 2004, pp. 26–31.

[23] R. W. Cernosek, S. J. Martin, A. R. Hillman, and H. L. Bandey, "Comparison of lumped-element and transmission-line models for thickness-shear-mode quartz resonator sensors," *IEEE Transactions on Ultrasonics, Ferroelectrics, and Frequency Control*, vol. 45, no. 5, pp. 1399–1407, Sept 1998.

[24] K. Martin, L. Ozcolak, Y. S. Lee, and G. C. Temes, "A differential switched-capacitor amplifier," *IEEE Journal of Solid-State Circuits*, vol. 22, no. 1, pp. 104–106, Feb 1987.

[25] J. L. Lai, T. Y. Lin, C. F. Tai, Y. T. Lai, and R. J. Chen, "Design a low-noise operational amplifier with constant-gm," in *Proceedings of SICE Annual Conference 2010*, Aug 2010, pp. 322–326.

[26] A. D. Marcellis, G. Ferri, and P. Mantenuto, "Uncalibrated operational amplifier-based sensor interface for capacitive/resistive sensor applications," *IET Circuits, Devices Systems*, vol. 9, no. 4, pp. 249–255, 2015.

[27] P. B. Basyurt, D. Y. Aksin, E. Bonizzoni, and F. Maloberti, "Sampled-data operational-amplifier with ultra-low supply voltage and sub uw power consumption," in *2014 IEEE International Symposium on Circuits and Systems (ISCAS)*, June 2014, pp. 1893–1896.

[28] A. Panigrahi and A. Parhi, "A 0.5v voltage-combiner based pseudo differential ota design in cmos using weakly inverted transistors," in *2016 IEEE International Symposium on Nanoelectronic and Information Systems (iNIS)*, Dec 2016, pp. 144–148.

[29] O. Mirmotahari, J. Lomsdalen, and Y. Berg, "A continuous mvl gate using pseudo floating-gate," in *2007 14th International Conference on Mixed Design of Integrated Circuits and Systems*, June 2007, pp. 185–188.

[30] O. Mirmotahari, Y. Berg, and A. H. Navin, "A reversible cmos ad / da converter implemented with pseudo floating-gate," *International Journal of Electrical, Computer, Energetic, Electronic and Communication Engineering*, vol. 2, no. 2, pp. 202 – 205, 2008. [Online]. Available: `http://waset.org/Publications?p=14`

[31] M. Azadmehr and Y. Berg, "A band pass auto-zeroing floating-gate amplifier," in *2011 Faible Tension Faible Consommation (FTFC)*, May 2011, pp. 83–86.

[32] Y. Berg, M. Azadmehr, O. Mirmotahari, and S. Aunet, "Band pass pseudo floating-gate amplifier," in *2007 14th IEEE International Conference on Electronics, Circuits and Systems*, Dec 2007, pp. 506–509.

[33] M. Azadmehr and Y. Berg, "An auto-zeroing current-starved floating-gate band pass filter," in *2010 4th International Symposium on Communications, Control and Signal Processing (ISCCSP)*, March 2010, pp. 1–4.

[34] ——, "Bi-directional band pass / band stop filter based on current-starved pseudo floating-gate inverters," in *2008 NORCHIP*, Nov 2008, pp. 114–118.

[35] M. Azadmehr, B. K. Khajeh, and Y. Berg, "An ultra-low voltage tunable dual-band pass filter," in *2014 IEEE 11th International Multi-Conference on Systems, Signals Devices (SSD14)*, Feb 2014, pp. 1–5.

[36] M. Azadmehr and Y. Berg, "Current-starved pseudo floating-gate filters," in *2009 6th International Multi-Conference on Systems, Signals and Devices*, March 2009, pp. 1–5.

[37] ——, "Cascade of current-starved pseudo floating-gate inverters," in *2008 15th IEEE International Conference on Electronics, Circuits and Systems*, Aug 2008, pp. 1030–1033.

[38] Y. Berg and M. Azadmehr, "Reconfigurable pseudo floating-gate analog circuits," in *2010 17th IEEE International Conference on Electronics, Circuits and Systems*, Dec 2010, pp. 211–214.

[39] M. Azadmehr and Y. Berg, "A bi-directional autozeroing amplifier for designing bi-directional time-continuous frequency mixer/extractor," in *TENCON 2009 - 2009 IEEE Region 10 Conference*, Jan 2009, pp. 1–4.

[40] O. Mirmotahari and Y. Berg, "Proposal for a bidirectional gate using pseudo floating-gate," in *4th IEEE International Symposium on Electronic Design, Test and Applications (delta 2008)*, Jan 2008, pp. 196–200.

[41] M. Azadmehr, Y. Berg, and O. Mirmotahari, "Bi-directional current-starved pseudo floating-gate differentiator / integrator," in *2008 15th IEEE International Conference on Electronics, Circuits and Systems*, Aug 2008, pp. 275–278.

[42] C. Hagleitner, D. Lange, A. Hierlemann, O. Brand, and H. Baltes, "Cmos single-chip gas detection system comprising capacitive, calorimetric and mass-sensitive microsensors," *IEEE Journal of Solid-State Circuits*, vol. 37, no. 12, pp. 1867–1878, Dec 2002.

Articles omitted from online edition due to publisher's restrictions

Article 1:
L. Marchetti, A. Romi, Y. Berg, O. Mirmotahari and M. Azadmehr, "A discrete implementation of a bidirectional circuit for actuation and read-out of resonating sensors," 2016 International Conference on Design and Technology of Integrated Systems in Nanoscale Era (DTIS), Istanbul, 2016, pp. 1-5. doi: 10.1109/DTIS.2016.7483896

Article 2:
L. Marchetti, Y. Berg, O. Mirmotahari and M. Azadmehr, "Bidirectional front-end for piezoelectric resonator," 2016 IEEE 13th International Conference on Networking, Sensing, and Control (ICNSC), Mexico City, 2016, pp. 1-4. doi: 10.1109/ICNSC.2016.7479028

Article 3:
L. Marchetti, Y. Berg and M. Azadmehr, "An autozeroing inverter based front-end for resonating sensors," 2017 12th International Conference on Design & Technology of Integrated Systems In Nanoscale Era (DTIS), Palma de Mallorca, 2017, pp. 1-5. doi: 10.1109/DTIS.2017.7930154

Article 4:
L. Marchetti, Y. Berg, O. Mirmotahari and M. Azadmehr, "A control system for a low power bidirectional front-end for resonating sensors," 2017 IEEE 14th International Conference on Networking, Sensing and Control (ICNSC), Calabria, Italy, 2017, pp. 322-326 . doi: 10.1109/ICNSC.2017.8000112

Article 5:
L. Marchetti, Y. Berg and M. Azadmehr, "A Bidirectional Front-End with Band- width Control for Actuation and Read-Out of MEMS Resonating Sensors," 2017 24th International Conference Mixed Design of Integrated Circuits and Systems (MIXDES), Bydgoszcz, 2017,

Article 6:
L. Marchetti, Y. Berg and M. Azadmehr, "Analysis of the E_ect of Channel Leakage on Design, Characterization and Modelling of a high voltage Pseudo-Floating Gate Sensor-Front-End", accepeted in Electronics MDPI journal

Article 7:
L. Marchetti, Y. Berg and M. Azadmehr, "Design and Modelling of a Bidirectional Front-End for Resonating Sensors based on Pseudo Floating Gate Ampli_er", ac- cepted in Electronics MDPI journal

Co-Author of the following publications:

Article 8:
M. Azadmehr, L. Marchetti, Y. Berg "A Low Power Voltage Similarity Circuit," 2017 IEEE 50th International Symposium of Circuits and Systems (ISCAS), Balti- more, 2017

Article 9:
M. Azadmehr, L. Marchetti, Y. Berg, "A Virtual Wheatstone Bridge Front-End for Resistive Sensors," 2017 IEEE 14th International Conference on Networking, Sens- ing, and Control (ICNSC), Calabria, 2017